Applied Geochemistry 207 (2026) 106962

Contents lists available at ScienceDirect

Applied Geochemistry

journal homepage: www.elsevier.com/locate/apgeochem

# Meromictic stratification and geochemical gradients in a flooded abandoned apatite and mica mine (Quebec, Canada)

Élisa Pastier [a,b], Élise Lhoste [c], David Jaclin [d], Cassandre Sara Lazar [c], Violaine Ponsin [a,b,*]

[a] Department of Earth and Atmospheric Sciences, Université du Québec à Montréal, Montreal, Quebec, Canada
[b] Geotop Research Centre, Montreal, Quebec, Canada
[c] Department of Biological Sciences, Université du Québec à Montréal, Montreal, Quebec, Canada
[d] Faculty of Social Sciences, University of Ottawa, Ottawa, Ontario, Canada

ARTICLE INFO

Editorial handling by: Elisa Sacchi

*Keywords:*
Flooded mine
Open-pit lake
Meromictic lake
Lake stratification
Stable isotopes
Geochemistry

ABSTRACT

Mining resources are important in Canada, which has led to many abandoned mines prior to the 1991 mining regulations. Flooded mines that do not pose immediate risks to the environment or human health remain understudied. This study investigates the hydrochemistry and density stratification of a flooded apatite and mica mine (an open pit lake connected to underground levels) in Quebec, focusing on depth-dependent gradients and seasonal variations. Vertical profiling revealed a meromictic structure consisting of three layers: an oxic mixolimnion extending to a depth of 8 – 9 m, a transition zone characterized by a thermocline and chemocline, and a permanently anoxic monimolimnion below 11 m. Seasonal variations were confined to the mixolimnion, whereas deeper water remained chemically and physically stable throughout the sampling period, from early May to the end of October. Stable water isotope data further support the stratification, with shallow samples showing evaporation, deep samples aligning with the Local Meteoric Water Line (LMWL), and very few intermediate data points. The open-pit morphometry, the steep slopes surrounding the lake, and density differences were very likely responsible for the development of meromixis. $\delta^{34}S–SO_4$ values indicate active microbial sulfate reduction in the chemocline and the anoxic monimolimnion, while the precipitation of carbonates and metal sulfides control the chemistry of the monimolimnion. Phosphorus and nitrogen accumulated in the mixolimnion following the establishment of stable water column stratification. These findings identify the Blackburn Mine as a valuable model for investigating hydrochemical and biogeochemical processes in flooded mica and apatite mines, and for improving our understanding of density and thermal stratification in subsurface aquatic environments.

## 1. Introduction

In Canada, mining holds both economical and historical importance. In the Quebec province, mining activities date back to the late 19th century and have included the extraction of metals such as gold, iron, and copper (Association Minière du Québec, 2022). In addition to metallic mining, non-metallic mineral extraction has also been widespread in Quebec, including the mining of mica and apatite, which have historically been exploited in several regions of the province (Gatineau Valley Historical Society (GVHS), 1998; Ministère des Ressources naturelles et des Forêts du Québec, 2026). Before the implementation of the 1991 restoration law (Ministère de l'Emploi et de la Solidarité Sociale (MTESS), 2024), mines were often abandoned without any rehabilitation effort. Subsequent flooding by groundwater led to the formation of new artificial subsurface aquatic environments, characterized by confined, dark and cold conditions colonised by specialised microbial communities (Keshri et al., 2015; Lhoste et al., 2023). In Quebec alone, as of 2025, 338 mines remained abandoned without any restoration plan, underscoring the widespread occurrence of unmonitored flooded mine sites (MRNF, 2025). The National Orphaned/Abandoned Mines Initiative (NOAMI), which operated from 2002 to 2022, was a Canadian initiative established to address issues related to orphaned and abandoned mines, provide recommendations for site management, and facilitate the implementation of remediation programs. Since 2022, it has since been succeeded by the Annual Orphaned and Abandoned Mines Workshop under the Canadian Minerals and

* Corresponding author. Department of Earth and Atmospheric Sciences, Université du Québec à Montréal, Montreal, Quebec, Canada.
*E-mail address:* ponsin.violaine@uqam.ca (V. Ponsin).

https://doi.org/10.1016/j.apgeochem.2026.106962
Received 11 December 2025; Received in revised form 25 June 2026; Accepted 25 June 2026
Available online 27 June 2026

Metals Plan (Government of Canada, Natural Resources Canada, 2026).

These sites are often highly heterogeneous due to variations in geology, hydrology, mining history, and human disturbance, making it difficult to predict their hydrochemical behavior and long-term evolution. While research on flooded mines has primarily focused on pollution and remediation of heavily contaminated sites, relatively unpolluted mines remain poorly studied, despite their potential to reveal long-term hydrochemical and biogeochemical processes. For instance, Atanacković et al. (2013) conducted a risk-based regional screening of 59 abandoned mine sites in Serbia to identify and rank those posing the highest risk for surface water contamination, thereby targeting restoration efforts based on hazard potential rather than purely on abandoned-mine inventory (Atanacković et al., 2013).

This general lack of hydrochemical and biogeochemical data is evident for non-metallic mines. In Canada, numerous mica occurrences have been documented, but only a limited number were mined. In Quebec alone, about 100 mica occurrences are recorded, yet only a few mines were active, including the Dacey and Blackburn mines at Cantley (also mined for apatite), the Compagnie du Saguenay, and the Château-Richer mines (Gatineau Valley Historical Society (GVHS), 1998; MRNF, n.d.; Le Echo de la Tuque, 2022; Phillips, 2017). The only mica mine still operating in 2025 is the Lac Letondal mine. In Ontario, roughly 30 mica occurrences are recorded, with mining starting in the late 19th century (Ontario Ministry of Northern Development, Mines and Forestry, n.d.). Very few studies have addressed post-flooding hydrochemical or biogeochemical processes on former mica or apatite mines. Available research typically focuses on geotechnical, mineralogical, or environmental management aspects. For example, Munnoch et al. (2011) investigated the implementation of a pit lake at the Agrium Kapuskasing Phosphate Operations after mine closure, combining geotechnical, geochemical, and biological approaches to assess the stability and evolution of the flooded pit lake (Munnoch et al., 2011). Chlahbi (2024) conducted a geomineralogical characterization of a sedimentary phosphate deposit in Morocco to improve waste management and valorization strategies (Chlahbi, 2024).

Previous studies have shown that flooded mines, including pit lakes, can develop seasonal or persistent stratification, similar to the layering observed in holomictic or meromictic natural lakes (Boehrer and Schultze, 2008; Castendyk and Eary, 2009; Mugova and Wolkersdorfer, 2022; Wetzel, 2001). Most natural lakes are holomictic and undergo at least one complete mixing of the water column per year, which periodically disrupts stratification and restores vertical homogeneity of temperature, dissolved oxygen and solutes (Boehrer and Schultze, 2008; Wetzel, 2001). In these lakes, stratification is generally seasonal and transient, controlled by climatic forcing. In contrast, in meromictic lakes, the water column is permanently stratified, with a surface mixolimnion overlying a deep monimolimnion that does not undergo complete seasonal mixing, allowing the persistence of long-term chemical and density gradients (Boehrer and Schultze, 2008; Fuchs et al., 2022). The mixolimnion is separated from the monimolimnion by pronounced thermoclines and chemoclines, and solutes tend to accumulate in the monimolimnion, which is often anoxic. Microbial communities play a central role in these environments, catalysing key reactions such as sulfate reduction or (di-)sulfide oxidation (Aelion et al., 2009; Gammons et al., 2014).

Examples of natural meromictic lakes include Lake Pavin (France) and Crawford Lake (Canada), which have been extensively studied and illustrate how stratification governs redox dynamics and controls hydrochemical cycles in natural settings (McCarthy et al., 2023; Olive and Boulègue, 2004; Omaly, 1968). Stratification has been reported in several flooded mines worldwide, often under acidic conditions. Notable examples include La Cueva de la Mora pit lake (Sánchez-España et al., 2009). In some cases, meromixis may develop or be maintained, either naturally or though management practices, to confine undesirable substances in deep water or to maintain specific conditions for water treatment (Castendyk and Eary, 2009).

This study aimed to characterise the stratification and seasonal dynamics of the flooded Blackburn open pit lake as a model for non-metallic mines (here: apatite and mica) in comparable geological and environmental contexts. More specifically, (i) the physical and hydrological factors controlling stratification and (ii) the distribution of dissolved elements were investigated. Finally, (iii) nutrient concentrations and primary productivity indicators were analyzed to assess the lake's trophic status.

## 2. Materials and methods

### 2.1. Study site

The Blackburn mine is located at the north of Gatineau-Ottawa, within the Blanche River West watershed in Canada, in a forested area (Fig. 1A). The site is located in the Grenville province, where the geological formations are metamorphosed skarns and calc-silicates; the assemblages of minerals found (pyroxenes, amphiboles, calcite, epidote or titanite) are typical of hydrothermal interactions in metamorphosed carbonate rocks (Meinert, 1992; Vernon, 2004). The mine site is associated with mineralized pyroxenite lenses related to calc-silicate rocks that crosscut a biotite paragneiss and are themselves crosscut by pegmatite (MRNF, 2026). The mine was initially exploited, starting in 1878, for fluorapatite as a source of phosphate for agricultural use. Subsequently, mining focused on phlogopite, which is a magnesium-rich biotite found in skarnic calcsilicates associated with carbonate rocks, for its insulating properties (Des mines et des hommes, 2012; Sabina, 1987; Spence, 1929). Mining activity ceased in 1942 (White, 1997). During operation, pumps were used to keep the mine dry, and once pumping stopped following mine closure, groundwater gradually flooded the excavations. Mineralogical inventories available for Blackburn also indicate the presence of accessory minerals such as calcite, diopside, actinolite, fluorite, graphite, and titanite, as well as minor sulfides like pyrite, in the associated calcsilicates and skarns (Sabina, 1987).

The subhumid, temperate climate is characterized by moderate annual precipitation and a seasonal snowmelt cycle (Comeau et al., 2013). Total rainfall and total snowfall between 2023 and 2025 were respectively: 735.2 mm and 203.7 cm at the station Ottawa CDA (Ontario, Canada) near the mine (SI, Fig. S1) (Government of Canada, 2023). Monthly mean temperature at the same station is below zero in winter and above 20 °C in summer. The snow cover remains for several months in winter, and water bodies in the region freeze seasonally.

The Projet d'Acquisition de Connaissances des Eaux Souterraines en Outaouais (PACES-OUT), which is a regional study of aquifers, indicates that aquifers are primarily unconfined and that the groundwater chemistry is dominated by the hydrogen carbonate (Ca–$HCO_3$) facies, reflecting the predominance of local carbonate formations (Comeau et al., 2013). There are no surface water inflows to or outflows from the open pit lake, although there are limited, temporary seasonal inflows linked to snowmelt, typically occurring between March and May. Several small water points observed near the mine, identified as vernal pools, are highly seasonal and are often dry during the summer, suggesting that their occurrence is related to snowmelt or spring precipitation. Local groundwater flow through the mine is from southeast to northwest.

There are no official maps of the mine showing the complete layout and connections between the different largely unexplored levels. Divers are involved in the project to collect samples and map the flooded Blackburn mine (both open pit lake and underground levels). Fig. 1 shows the location of the mine, along with the surface water bodies and private wells from which samples were collected (Fig. 1B). The mine cross-section, based on the diver's surveying, shows an open pit with steep slopes, approximately 104 m in length and 63 m in width, with a water surface area of 2,400 $m^2$ and a pit depth of 30 m. The water level is approximately 12 m below ground surface. A level extends from the pit and splits into two branches, descending to depths of 52 and 59 m,

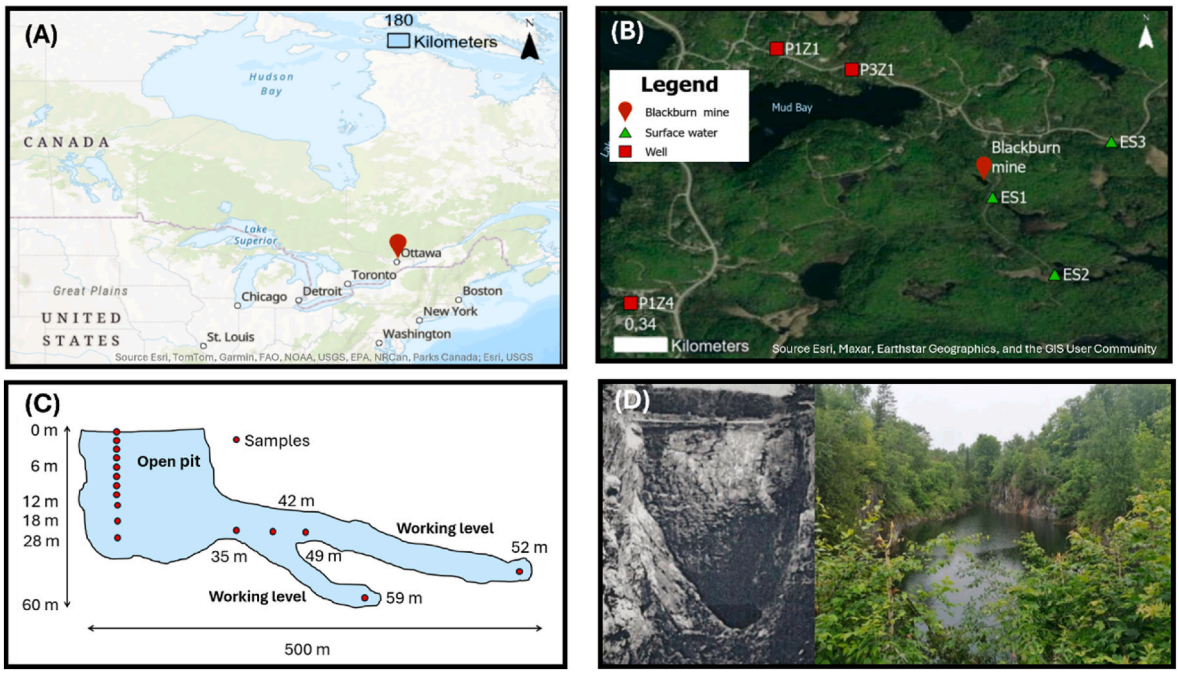


**Fig. 1.** (A) location of the mine in Canada (red marker), (B) location of the sampling points: mine, surface water (green triangles) and private wells (red squares). The maps were generated with ArcGIS Pro (ESRI, 2024, v 3.1). (C) cross-section of the mine showing sampling depths and (D) pictures of the mine during exploitation in 1912 (Spence, 1929) (left) and after exploitation in 2023 (right). (For interpretation of the references to color in this figure legend, the reader is referred to the Web version of this article.)

respectively (Fig. 1C and D). Thus, the Blackburn mine is not a characteristic pit lake, as it is hydraulically connected to additional underground levels, and could serve as a relevant analogue for the studying of similar flooded open pit lakes.

### 2.2. Sampling

A Levelogger (Solinst®, Levelogger 5, Junior, model 3001) and a Barologger (Solinst®, Barologger 5, model 3001) were installed from June 30 to October 30, 2023, from May 12 to October 30, 2024, and from May 8 to October 18, 2025. Their function was to record hourly water level variations in the flooded open pit lake (daily averages reported). No direct barometric pressure data were collected in 2024 because the barologger was stolen; therefore, 2024 pressure variations were estimated using data from a nearby meteorological station (the methodology and reconstructed dataset are provided in the Supporting Information).

Sampling depths were defined relative to the water surface. Samples from the pit lake were taken using a Van Dorn bottle (Wildco® Instruments, Beta Bottle 2.2 L) for depths between 0 and 12 m (one sample every 1.5 m) (Fig. 1C). Samples at the bottom of the pit lake and at various depths (18, 30, 37, 43 and 52 m) were collected by divers with 200 mL plastic syringes (Fig. 1C), during the descent and after sampling with the Van Dorn bottle was completed. Divers used closed-circuit rebreathers, preventing any contamination of the water samples. Samples were collected once per season, from early May (spring) to late October (autumn) between 2023 and 2025. Sampling dates and associated analyses are shown in the Supporting Information (Table S1). There was no sampling between November and April for safety reasons (access covered by snow and ice). Samples for water isotopes were taken between 0 and 12 m (one sample every 1.5 m), 18, 30, 37, 43 and 52 m in summer and autumn 2024, but from 18 m in spring of 2024 due to a sampling issue. Additional samples were collected in spring 2025 at all depths to complete the dataset. A duplicate was taken every fifteen samples on average, i.e. one duplicate per field trip. Samples from three nearby surface water points (ES1, ES2 and ES3) were collected just below the water surface once per season for major cations, anions and alkalinity analyses in 2023 and 2024 (Fig. 1B). Three nearby private wells (P1Z1, P3Z1 and P1Z4) were also sampled in autumn of 2024 for the same parameters and for sulfate isotopes (Fig. 1B). Physicochemical parameters (temperature, pH, electrical conductivity [EC] and dissolved oxygen [DO] were recorded in the field using a multiparameter probe equipped with integrated temperature, pH, EC (automatically adjusted to 25 °C) and DO sensors (WTW Multi 3630 IDS) for samples taken with the Van Dorn bottle (from 0 to 18 m). A HOBO probe (ONSET U-DTW-1 HOBO, Onset Computer Corporation, USA) attached to the belt of one diver was used to continuously measure temperature and DO during dives (one reading per minute). Details about calibration are provided in SI (section 2.2). To ensure the consistency of oxygen data from the two probes, measurements were compared for the same sampling campaign. Water samples were filtered in the field using 0.45 µm polyethersulfone filters (Sarstedt®, Numbrecht, Germany) except for ammonium samples, which were filtered through 0.2 µm polyethersulfone filters (Sarstedt®, Numbrecht, Germany) and stored frozen until analysis. Samples for cation analysis were acidified immediately after collection with 10% nitric acid (1 drop per 10 mL of sample) to prevent metal precipitation and maintain cation concentrations in solution. For sulfide ion measurements, approximately 0.15 mL of 1.2 mol/L zinc acetate solution and 0.03 mL of 1 mol/L sodium hydroxide solution were added for preservation of 25 mL samples (Centre d'expertise en analyse environnementale du Québec (CEAEQ), 2023). Dissolved total nitrogen (TN, DN, NOx, $NO_2$, $NO_3$) and dissolved total phosphorus (TP, DP, $PO_4$, P) were preserved in borosilicate glass tubes (25 × 150 mm, Corning PYREX®, Fisher Scientific, Cat. No. 14-933D) sealed with PTFE caps (25 × 150 mm, Fisher 14-933D). Chlorophyll *a* (Chl *a*) samples were collected using a 12 V submersible pump (model 3262, serial number 12 V, PU/PS, Geneq) and immediately filtered in the field through GF/F filters (0.7 µm). Water transparency was assessed using a 20 cm diameter Secchi disk on September 20, 2025, at 10:30 a.m., and the depth of visibility was recorded in meters. Samples for sulfate isotope analysis were collected at the open pit lake and from the three wells before being filtered in an anaerobic chamber (810-SG Series by

PLAS-LAB S atmosphere composition: 85% nitrogen, 10% hydrogen and 5% carbon dioxide) to avoid oxygen contamination. Sediments were collected in June 2022 at 52 m at the bottom of the sampled level (Fig. 1A), then frozen, before being filtered on a 0.2 μm polyethersulfone filter. The filter was then dried for 24 h in an oven at 40 °C for energy-dispersive X-ray fluorescence (XRF) analysis.

### 2.3. Analyses

#### 2.3.1. Hydrochemical analyses

Anions (fluoride, chloride, nitrite, nitrate, phosphate and sulfate) were analyzed within 48 h of collection by ion chromatography (Dionex Aquion, Thermo Scientific, Waltham, MA, USA) at the GEOTOP-UQAM laboratory. Ion separation was achieved using an anion exchange column (Dionex IonPac AS22) and carbonate/bicarbonate eluent (Thermo Scientific™ Dionex™ AS22 carbonate/bicarbonate solution, 1/100 dilution). Nine standards were used ranging from 0.1 to 100 mg/L. A Certipur multi-element standard was included in each sequence to check the accuracy of calibration. Major cations ($Ca^{2+}$, $Mg^{2+}$, $Na^{+}$, $K^{+}$) were analyzed by an inductively coupled plasma optical emission spectrometer (ICP-OES, Agilent Technologies 5100) at the NanoQAM laboratory. Multi-element standards from Inorganic Ventures' "Groundwater & Wastewater (Alternate Metal) Standards" range, prepared in matrix solution at 2% $HNO_3$ were used. Calibration standards cover a concentration range from 0.01 to 500 mg/L depending on the measured elements. Limits of detection and quantification have been determined for each element and are summarized in SI (Table S1). Standard checks and blanks were incorporated into each sequence. Alkalinity was measured within 48 h of collection by an automatic potentiometric titrator (Hanna Instruments, model HI 902 Color) with 10% hydrochloric acid at the GÉOTOP-UQAM laboratory. Alkalinity was measured in meq/L and then converted to mg/L as $CaCO_3$ equivalent. Sulfide ion measurements were made by a field spectrophotometer (programme 690, HACH DR2800, Hach Company, 2007) using a colorimetric method based on methylene blue formation with absorbance measured at 664 nm (Matheson, 1974). Concentrations of sulfide ion should be considered semi-quantitative estimates only. Concentrations are reported as follows: nitrite as $NO_2^-$; nitrate as $NO_3^-$; phosphate as $PO_3^{4-}$; sulfate as $SO_4^{2-}$, sulfide ion as $S^2$ and Ammonium as $NH_4^{+}$. XRF analysis was performed by a portable XRF analyzer (ThermoScientific, model Niton XL3t Goldd+). The analysis mode was AllGeo with a total duration of 120 s, 30 s for each analysis window: Main, Low, High and Light Range allowing to cover a wide range of elements, from the lightest to the heaviest, in a single measurement. The instrument was calibrated using Standard Reference Materials (SRM, list available in SI, section 2.3.), and all reported concentrations were calculated following this calibration.

#### 2.3.2. Trophic state indicators

Analyses of total nitrogen (TN), total phosphorus (TP), and Chl *a* were performed at the GRIL-UQAM laboratory following their internal protocols. TN was measured using a continuous flow analyzer (OI Analytical Flow Solution 3100®) following the standard alkaline persulfate digestion method coupled with Cd reduction and colorimetric detection (using US EPA Method 353.2 (Patton and Kryskalla, 2003)). Analytical precision was <5% for a concentration range of 0.005 – 10 mg/L. TP was determined after potassium persulfate digestion (121 °C, 20 min) and quantified spectrophotometrically (890 nm, Ultrospec 3100pro, Amersham Biosciences) following the standard method (Bridgewater et al., 2017). Analytical precision was <5% for a concentration range of 0.005 – 10 mg/L. Chl *a* was extracted in 90% ethanol under both hot and cold conditions, and quantified by fluorometry (TD-700, Turner Designs; Ex 436 nm, Em 680 nm) and spectrophotometry (Ultrospec 3100pro, Amersham Biosciences). Trophic State Index (TSI) values were calculated following Carlson (1977) using total phosphorus (TP, μg/L), Chl *a* (μg/L), and Secchi depth (m) (Carlson, 1977). TP and Chl *a* were used to compute depth-specific TSI values within the photic zone (0 – 5 m), while Secchi depth provided a single surface-based index. TSI values were calculated for individual depths to capture vertical variations in nutrient and algal distribution. Limits of detection and quantification are provided in the Supporting Information (SI, Table S2).

#### 2.3.3. Stable isotopes of water and sulfate

Oxygen ($\delta^{18}O$) and sulfur ($\delta^{34}S$) isotopes in sulfate were measured with an elemental analyzer coupled to an isotope ratio mass spectrometer (EA-IRMS, Isoprime, GV Instruments) at the Environmental Isotope Laboratory (University of Waterloo). Prior to analysis, sulfate was quantitatively precipitated as barium sulfate ($BaSO_4$), following a well-established protocol to ensure purity and accuracy in isotope measurements (Révész et al., 2006/2012). For sulfur isotopes, solid samples were subjected to high-temperature pyrolytic combustion (1440 °C), converted to $SO_2$ and measured spectrometrically (Hunsinger et al., 2013). Oxygen isotopes were measured following pyrolytic conversion to $CO_2$. The standards used were internationally certified reference materials (IAEA–SO–5: 0.5 ± 0.2‰, IAEA–SO–6: −34.1 ± 0.2‰, NBS-127: 21.1 ± 0.4‰, for $\delta^{34}S$; IAEA-600: −3.5 ± 0.5‰, NBS-127: 9.3 ± 0.4‰, IAEA-601: 23.1 ± 0.2‰, IAEA-602: 71.3 ± 0.4‰ for $\delta^{18}O$). Standards were incorporated every 5 samples to correct instrumental drifts and ensure data reliability. Results were expressed using the delta notation ($\delta$) as follows (Equation (1)):

$$\delta\,(‰) = \left(\frac{R\text{sample}}{R\text{standard}} - 1\right) \times 1\,000 \qquad \text{(Equation 1)}$$

where R is the ratio of heavy to light stable isotopes (for example, $^{34}S/^{32}S$ for sulfur, $^{18}O/^{16}O$ for oxygen) for samples and standards, respectively. Values are reported in ‰ relative to the Vienna Canyon Diablo Troilite (VCDT) scale for sulfur and in ‰ relative to Vienna Standard Mean Ocean Water (VSMOW) scale for oxygen, with analytical precision better than 0.3‰ and 0.2‰ respectively.

The isotope fractionation ($\varepsilon$) value for sulfur was obtained from the slope of the linearized Rayleigh equation (Equation (2)):

$$\ln\left(\frac{\delta_x + 1}{\delta_0 + 1}\right) = \varepsilon \times ln\left(\frac{C_x}{C_0}\right) \qquad \text{(Equation 2)}$$

Where the initial conditions ($C_0$ and $\delta_0$) were defined from the least enriched sample—assumed to represent the starting composition of the studied environment —$\delta_x$ and $C_x$ represent the concentration and isotope value at depth $x$, and $\varepsilon$ is the enrichment factor. The reported error for $\varepsilon$ corresponds to the 95% confidence interval (*CI*) of the linear regression in the Rayleigh plot (Clark and Fritz, 1997).

Water stable isotopes ($\delta^{18}O$ and $\delta^{2}H$) were measured to assess mixing of the water column and evaporation (Wolkersdorfer et al., 2020). Measurements were done with an isotope ratio mass spectrometer coupled to an AquaPrep system (Isoprime, Micromass) in dual injection mode at the GEOTOP-UQAM laboratory. Water samples (200 mL) were transferred to sealed vials and heated to 40 °C. A hydrophobic platinum catalyst (Hokko beads) was added for $\delta^{2}H$ analysis, while the air in the vials was replaced by $CO_2$ or $H_2$ depending on the isotope to be analyzed. Samples were then left to equilibrate for 7 h for $\delta^{18}O$ and 4 h for $\delta^{2}H$. Calibration was based on three certified internal standards normalized to the VSMOW2-SLAP2 ($\delta^{18}O = 0.8 \pm 0.1‰$, $-14.4 \pm 0.4‰$ and $-25.7 \pm 0.1‰$; $\delta^{2}H = 5.5 \pm 0.5‰$, $-102.3 \pm 0.4‰$ and $184.9 \pm 0.8‰$). Additionally, a fourth standard was used as an unknown to assess analytical precision ($\delta^{18}O = -7.2 \pm 0.1‰$ and $\delta^{2}H = -52,8 \pm 0.9‰$). The associated uncertainties were better than ±0.1‰ for the $\delta^{18}O$ and ±2.0‰ for the $\delta^{2}H$, corresponding to a repeatability of one sigma over three analytical replicates. A local evaporation line (LEL) was calculated using a linear regression between $\delta^{2}H$ and $\delta^{18}O$ values using all data for 2024 (equation (3)):

$$\delta^2H = a \times \delta^{18}O + b \quad \text{(Equation 3)}$$

Where $a$ is the slope and $b$ is the intercept of the regression line.

### 2.4. Statistics and softwares

All statistical analyses and graphics were prepared with the RStudio environment (RStudio Team, 2024) on R v.4.3.2 (R Core Team, 2023). The complete list of packages used in this study is available in SI (section 3). Statistical analyses were performed to examine relationships between chemical parameters and with depth, considering the non-parametric nature of the data (Shapiro-Wilk tests showed significant deviations from normal distribution). A PERMANOVA was used to test for significant differences between data groups, defined according to season (spring, summer, autumn), DO concentration, depth and depth groups (0 – 4 m, 5 – 15 m, >15 m). Spearman's rank correlation tests were used to assess the relationship between two variables and to identify general trends. A redundancy analysis (RDA) was conducted to explain variations in chemical variables based on environmental variables such as depth, season or DO concentration. Differences were considered statistically significant at the $\alpha = 0.05$ confidence level. The DIAGRAMMES (v 8.1) software (Roland Smiller, Université d'Avignon, France) was used to create Piper diagrams, calculate ion balances (%) and concentrations of total dissolved solids (TDS in mg/L) (Piper, 1944, 1953). Alkalinity was converted to mg/L of $HCO_3^-$ for the Piper Diagram, ion balances and TDS concentrations. Ion balances were calculated as the percent difference between cation and anion equivalents to verify charge neutrality, while TDS concentrations were estimated as the sum of the major dissolved ions, representing an operational proxy for TDS rather than an accurate measurement. Water density was estimated as a function of the measured water temperature and EC, using Thermodynamic Equation of Seawater (2010) (TEOS-10) (McDougall and Barker, 2011). Details about density estimation are provided in supporting information (Section 2.4).

The PHREEQC (v.3.7.3; 2023) chemical modeling software developed by the United States Geological Survey (USGS) was used to calculate saturation indices of phases, using the phreeqc.dat database provided with the software (Parkhurst and Appelo, 2013). Calculations

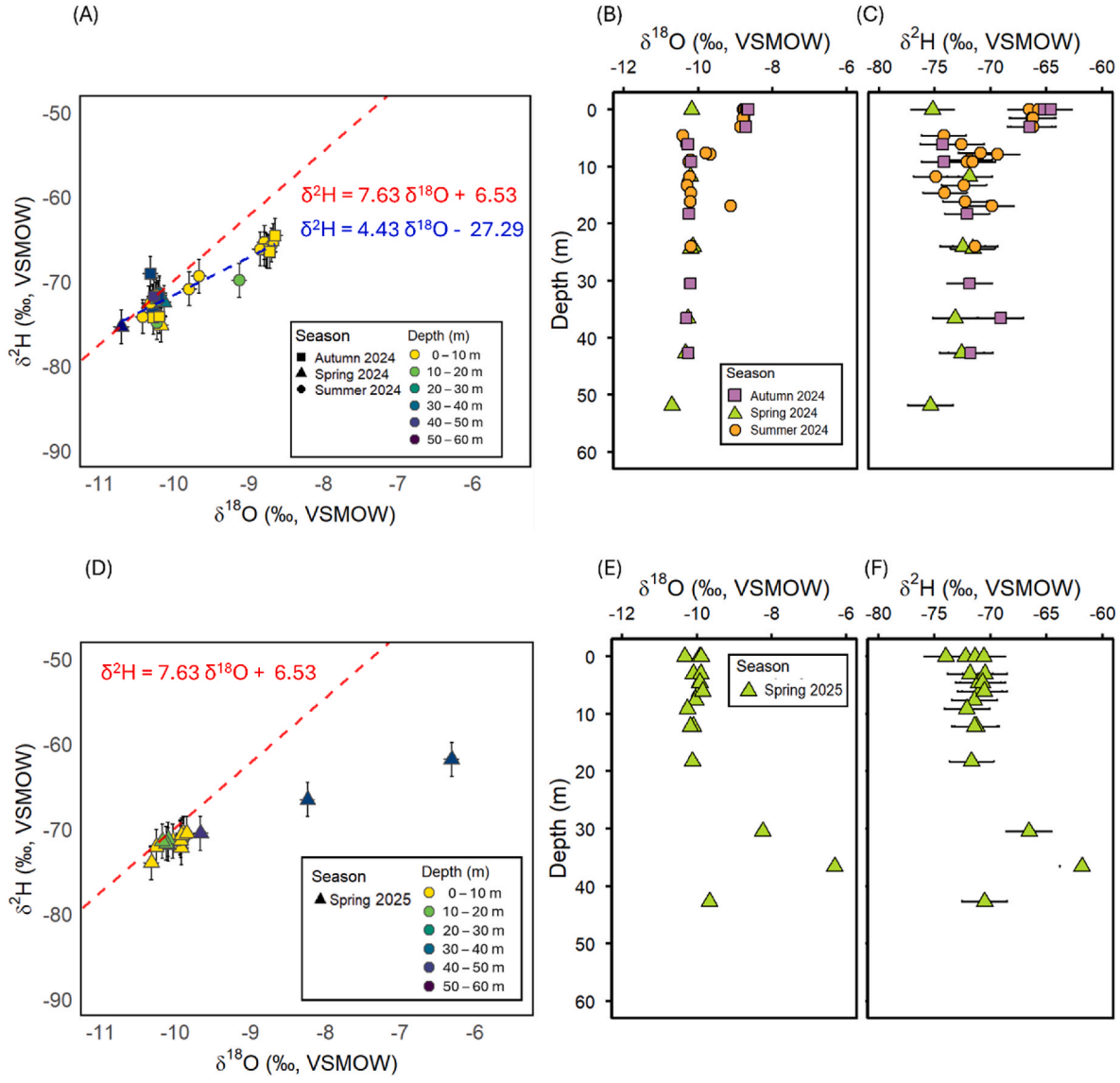


**Fig. 2.** Isotope values of mine water in 2024 (A, B and C) and in 2025 (D, E and F) for spring (triangle), summer (circle), and autumn (square) following a color gradient based on depth from shallowest (yellow) to deepest (dark blue) (A and D) and as a function of depth (B, C, E and F). The red line represents the Local Meteoric Water Line for the Ottawa River Basin (Telmer and Veizer, 2000). The blue line represents the Local Evaporation Line in 2024 ($R^2 = 0.86$). (For interpretation of the references to color in this figure legend, the reader is referred to the Web version of this article.)

were done for two depths, 8 and 37 m, using the S(-II)/S(VI) couple to estimate pe.

## 3. Results

As concentration profiles and ranges along the water column were similar between 2023 and 2025, only the 2024 results are described and later discussed. Results from other years are presented and discussed only when they differ from those of 2024 and are summarized in the SI (Table S3).

### 3.1. Water level and water isotopes

A water level probe installed in the flooded open pit recorded little variations in water level between July and mid-August 2023, but the level then steadily dropped by 0.7 m from the initial level until the probe was removed mid-October (SI, Fig. S2). Water level recordings from 2024 showed a similar seasonal pattern, despite slightly higher short-term variability associated with the use of reconstructed atmospheric pressure data (SI). Water level recordings from the open pit lake in 2025 showed that the drop in water level started earlier (late May), and by the time the probe was removed mid-October 2025, the water level had dropped by approximately 1.5 m.

For both 2024 and 2025, water isotope values in the mine spanned a narrow range of values. $\delta^{18}O$ values in 2024 ranged from −10.7 to −8.7‰ and $\delta^{2}H$ ranged from −75.4 to −64.7‰ (Fig. 2A–C; the abnormally heavy sample at 18 m in summer 2024 is probably due to an improperly capped bottle). Surface samples (0 – 5 m) were generally enriched in heavy isotopes ($\delta^{18}O$: −9 to −8.5‰; $\delta^{2}H$: −68 to −63‰), while deeper water (30 – 50 m) was depleted ($\delta^{18}O$: −10.7 to −10‰; $\delta^{2}H$: −75.4 to −69‰) across all seasons. Intermediate depths (7 – 17 m) exhibited transient values slightly below the local meteoric water line for the Ottawa River basin water (Fig. 2A) (Telmer and Veizer, 2000). A local evaporation line (LEL) was calculated using all $\delta^{2}H$ and $\delta^{18}O$ collected in 2024. The slope in 2024 was 4.43 ($R^2 = 0.86$).

In spring 2025, $\delta^{18}O$ values ranged from −10.7 to −6.3‰ and $\delta^{2}H$ from −75.4 to −61.8‰ (Fig. 2D–F). Vertical profiles revealed reversed stratification compared to 2024: surface water was isotopically lighter ($\delta^{18}O$: −8.2 to −6.3‰; $\delta^{2}H$: −74.2 to −70.5‰), while deeper water (>30 m) was heavier ($\delta^{18}O$: −10.3 to −9.7‰; $\delta^{2}H$: −66.6 to −61.8‰) (Fig. 2D–F).

### 3.2. Hydrochemical facies, TDS concentrations and density

Ion balances for mine water samples in 2024 ranged from −14 to −2%. Four samples out of 56 had ion balances below −15% or above 15% and their alkalinity measurements were inconsistent with the mean values of other samples at the same depth, therefore, they were not considered further. Mine water samples showed an average standard deviation of 5.4% for alkalinity, 9.6% for anions, 14.1% for sulfide ion, 16.1% for cations, 0.9% for water isotopes and 7.4% for sulfate isotopes, indicating a narrow range of variation. Mine water, as well as surface water (ES1, ES2 and ES3) and groundwater from private wells (P1Z1, P3Z1 and P1Z4), exhibited a chemical facies dominated by calcium and hydrogen carbonate ions (SI, Fig. S3). However, one surface site, ES2, was an exception with higher concentrations of sulfate and chloride ions. TDS concentrations in 2024 for surface water samples (ES1, ES2 and ES3) ranged from 27 to 105 mg/L, while groundwater samples (P1Z1, P3Z1 and P1Z4) had TDS concentrations comprised between 417 and 595 mg/L in 2024 (SI, Table S3–S5). Median annual TDS concentrations and mean density in mine water in 2024 increased with depth. Surface TDS concentrations was 229 mg/L and increased slightly to 249 mg/L at 1.5 m, then rose progressively with depth, reaching 410 mg/L at 43 m. Density showed a comparable increase with depth, from 999.82 kg/m$^3$ at the surface to 1000.14 kg/m$^3$ at 4.5 m, remained relatively stable between 4.5 and 24 m in the open pit lake (1000.10 – 1000.21 kg/m$^3$) and reached 1000.19 kg/m$^3$ at 43 m in the working levels. (SI, Table S6).

### 3.3. Dissolved oxygen, temperature, electrical conductivity and pH

Dissolved oxygen (DO) and temperature data recorded by the probe attached to the diver's belt in 2024 were compared with dive profiles obtained from a personal dive computer, which tracks depth and time graphically. This allowed depth-dependent profiles to be created. Data from the ascent were used in the figures, as decompression stops provided multiple measurements at the same depth. Prior to measurements, the probes were allowed to equilibrate in the water to ensure signal stabilisation. To ensure consistency between the two approaches, HOBO probe data were compared with those from the multiparameter probe collected during the same day (SI, Fig. S4). Results were quite similar, with only a slight temperature difference (a few degrees in the first 5 m, likely due to different sampling times) and one lower DO concentration at 5 m with the HOBO probe. The HOBO probe was preferred because it provided more complete depth coverage. Temperature profiles in 2024 showed seasonal variations at the surface: between 7 and 11 °C during spring and autumn, and up to 16 °C in summer. At around 5 m depth, temperature dropped to 5 – 8 °C and remained stable at 5 – 6 °C below 10 m throughout the year (Fig. 3A). EC was 200 µS/cm at the surface and increased to 400 µS/cm at 5 m in all seasons in 2024. An exception was observed in spring, when one surface EC value reached 400 µS/cm (Fig. 3B). EC remained stable between 5 and 30 m, but in the working level (>30 m), it increased from 400 to 700 µS/cm in spring and autumn (no data for summer). pH ranged from 7 to 8 at the surface, decreasing to 6.5 – 7.5 in around 6 m depth, and remained stable below this depth (Fig. 3C). Seasonal differences were moderate, with pH differences of less than 1 unit between seasons. For example, at 10 m depth, mean pH values were 7.3 in spring, 7.0 in summer and 6.7 in autumn 2024.

### 3.4. Distribution of electron acceptors and dissolved species

HOBO probe profiles in 2024 showed surface DO concentrations of 10 mg/L in spring, 8 mg/L in summer, and 5 mg/L in autumn (Fig. 3D). DO decreased rapidly with depth. In spring, at 5 m, DO increased to 16 mg/L, while in summer and autumn, it dropped to 2.5 mg/L. Below 5 m, DO was undetectable in all seasons. Nitrite and nitrate concentrations were always below detection limits (LOD of 0.005 and 0.12 mg/L, respectively). Dissolved manganese was also undetectable at the surface (LOD = 0.01 mg/L) and was around 0.13 mg/L between 10 and 40 m and increased to 0.3 mg/L in the working level, with no seasonal variation (Fig. 3E). Total iron was below the detection limit at the surface (LOD of 0.01 mg/L), increased from 0.03 to 0.1 mg/L between 5 and 30 m, reaching 0.15 mg/L in the working level and at 52 m, concentration was 2 mg/L. As with manganese, no seasonal variations were observed (Fig. 3F). Sulfate concentrations were 15 mg/L from the surface to 5 m, decreased to 3 mg/L between 5 and 10 m, and remained stable at this concentration down to 30 m. Below 30 m (working level), sulfate was always below detection limits (Fig. 3G). Sulfide ions were below detection limits at the surface but ranged from < LOD to 1.5 mg/L below 10 m (Fig. 3H). Water samples taken between 6 and 10 m released a rotten-egg odour, consistent with the presence of hydrogen sulfide. Alkalinity concentrations were 150 mg/L $CaCO_3$ equivalent at the surface, increased to 230 mg/L at 10 m,remained stable down to 40 m depth, and finally increased slightly to >300 mg/L in the working level (>40 m) (Fig. 3I). No seasonal variations were observed. Major cations (Ca, Mg, K, Na) showed the same pattern of concentrations increasing with depth (SI, Fig. S5). For example, magnesium was 7 mg/L at the surface, 11 mg/L at 10–40 m and increased up to 15 mg/L > 40 m (SI, Fig. S5A). Concentrations of trace elements were generally low (SI, Table S3–S5). Fluoride concentrations ranged from 0.1 to 0.7 mg/L, increasing with depth (SI, Fig. S5E). Phosphate concentrations in 2024 were below the detection limit at the surface (LOD = 0.017 mg/L),

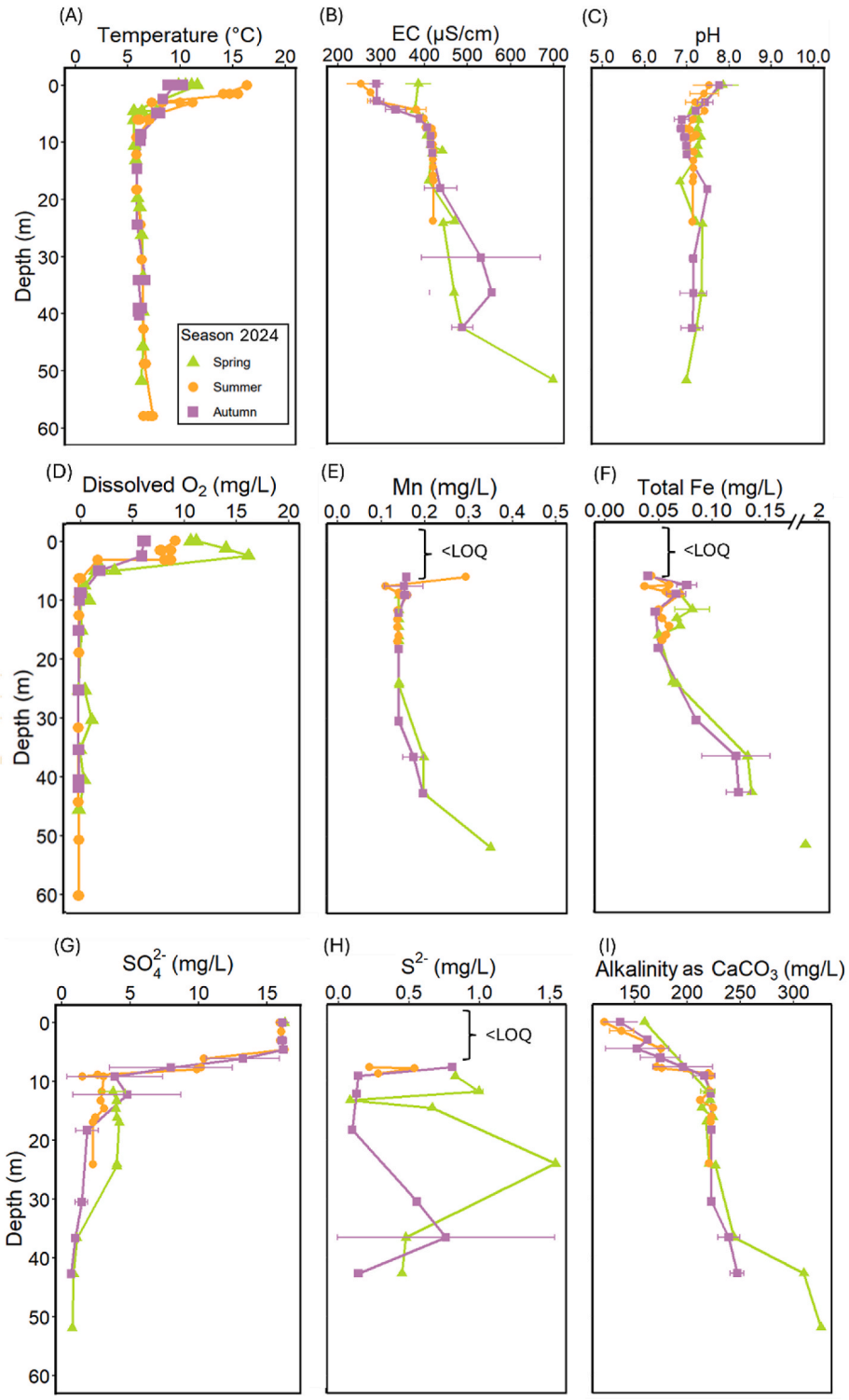


**Fig. 3.** Physicochemical parameters and concentrations as a function of depth: (A) temperature in °C and (D) DO in mg/L from the Hobo: 11 May 2024 (spring: triangle), 8 September 2024 (summer: circle) and 27 October 2024 (autumn: square). Seasonal mean value in 2024 for (B) EC in µs/cm, (C) pH ($n_{spring}$: 9; $n_{summer}$: 7; $n_{autumn}$: 13) and dissolved elements in mg/L: (E) manganese ($n_{spring}$: 9; $n_{summer}$: 6; $n_{autumn}$: 10), (F) total iron ($n_{spring}$: 9; $n_{summer}$: 6; $n_{autumn}$: 10), (G) sulfate as $SO_4^{2-}$ ($n_{spring}$: 10; $n_{summer}$: 7; $n_{autumn}$: 12), (H) sulfide ion as $S^{2-}$ ($n_{spring}$: 10; $n_{summer}$: 7; $n_{autumn}$: 7) and (I) alkalinity as $CaCO_3$ equivalent ($n_{spring}$: 10; $n_{summer}$: 7; $n_{autumn}$: 10).

reached 0.1 – 0.5 mg/L between 10 and 15 m, and 0.6 mg/L in the working levels. Concentrations were lower in summer and higher in autumn but followed the same depth-dependent pattern (SI, Fig. S5F).

### 3.5. Indicators of trophic status

Total phosphorus (TP), total nitrogen (TN), and ammonium concentrations were low at the surface and increased markedly with depth, particularly below 5 m (Fig. 4A, B and C). TP increased from approximately 100 µg/L at the surface to nearly 300 µg/L at 40 m, while TN

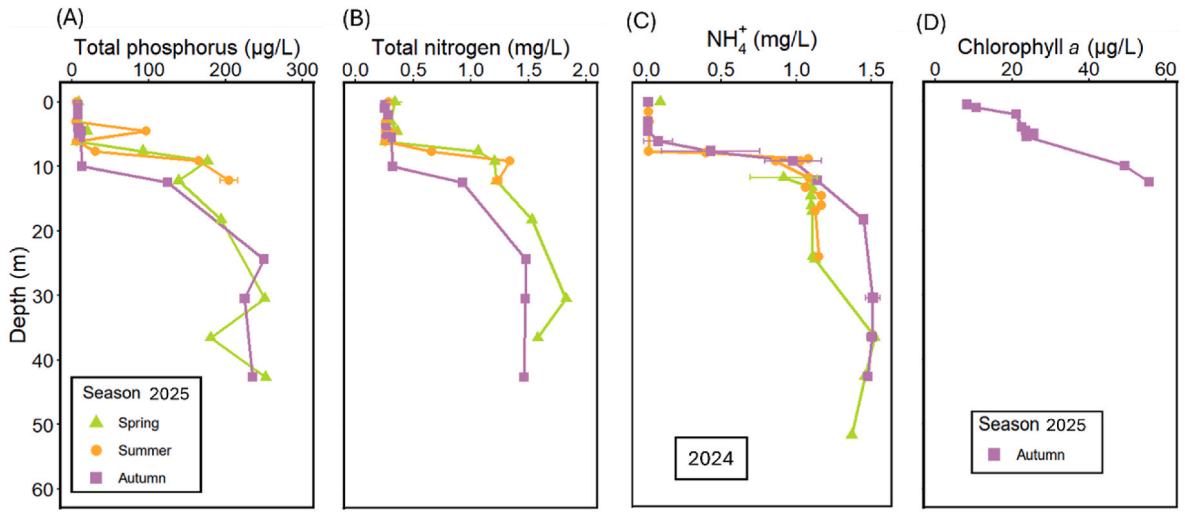


**Fig. 4.** Seasonal mean concentrations as function of depth: (A) total phosphorus in µg/L in 2025 ($n_{spring}$: 12; $n_{summer}$:13; $n_{autumn}$: 13), (B) total nitrogen in mg/L in 2025 ($n_{spring}$: 12; $n_{summer}$: 13; $n_{autumn}$: 13), (C) ammonium as $NH_4^+$ in mg/L in 2024 ($n_{spring}$: 14; $n_{summer}$: 21; $n_{autumn}$: 26) and (D) concentrations of chlorophyll *a* in µg/L in 2025 ($n_{autumn}$: 9).

increased from less than 1 mg/L in the 0 – 5 m range to almost 2 mg/L below 5 m (Fig. 4A and B). Ammonium concentrations remained low (<0.2 mg/L) at the surface but exceeded 1 mg/L at 10 m (Fig. 4C). Conversely, Chl *a* increased with depth, from near zero at the surface to nearly 60 µg/L at around 10 m (Fig. 4D). On average, the Secchi disk disappeared at 5 m. Trophic Status Index values were calculated for each depth from 0.5 to 12.5 m using TP, TN, and Chl *a*, Secchi disk measurements. TSI increased with depth, ranging from 56 in the surface to 82, with a mean of 63 across the profile (SI, Table S7).

### 3.6. Sulfate sulfur and oxygen isotopes

$\delta^{34}S$ and $\delta^{18}O$ values measured in mine water and groundwater ranged from 2.0 to 7.0‰ and from −1.9 to 3.3‰, respectively (Fig. 5A – B and Fig. S6), and an inverse correlation was observed between sulfate concentrations and $\delta^{34}S$ values in mine water, although the increase was limited for $\delta^{34}S$ values (5.2 – 7.0‰). $\delta^{18}O$ values did not show any specific trend with decreasing sulfate concentrations. Well samples displayed $\delta^{34}S$ and $\delta^{18}O$ values within the same range as the open pit and mine water, with only minor variations (Fig. S6A). The enrichment factor determined from $\delta^{34}S$ values for mine water samples was −2.4 ± 0.5‰ (Fig. 5C).

### 3.7. Sediments composition and PHREEQC simulations

XRF analyses revealed that the most abundant elements were Si, Ca, Fe, S, Mg, P, K and Al (approximate weight >1%, Table 1). Other detected elements in lake-sediment samples included for example Ti, Cl, Mn, Zr, Ba, Sr, Cr and Zn, all at trace concentrations (approximate weight <0.2%). The sediments collected in the working levels showed a black colour.

PHREEQC modelling allowed the calculation of redox potential (pe) and the saturation indices of different mineral phases at depths of 8 and 36 m. The pe values were estimated from the initial composition of the samples, using the S(-II)/S(VI) couple, and were below −3 for both depths. Calcite ($CaCO_3$) was close to equilibrium across the water column, with SI comprised between −0.5 (8 m) and 0.2 (36 m). In contrast, siderite ($FeCO_3$) and rhodochrosite ($MnCO_3$) were undersaturated at both depths with SI values of −1.3 and −0.7 for $FeCO_3$ and -0.7 and −0.1 for $MnCO_3$. Sulfide minerals such as pyrite ($FeS_2$) and mackinawite (FeS) were supersaturated at all depths (SI > 1). Hydroxyapatite ($Ca_5(PO_4)_3(OH)$) was undersaturated at 8 m (−3.8) and supersaturated

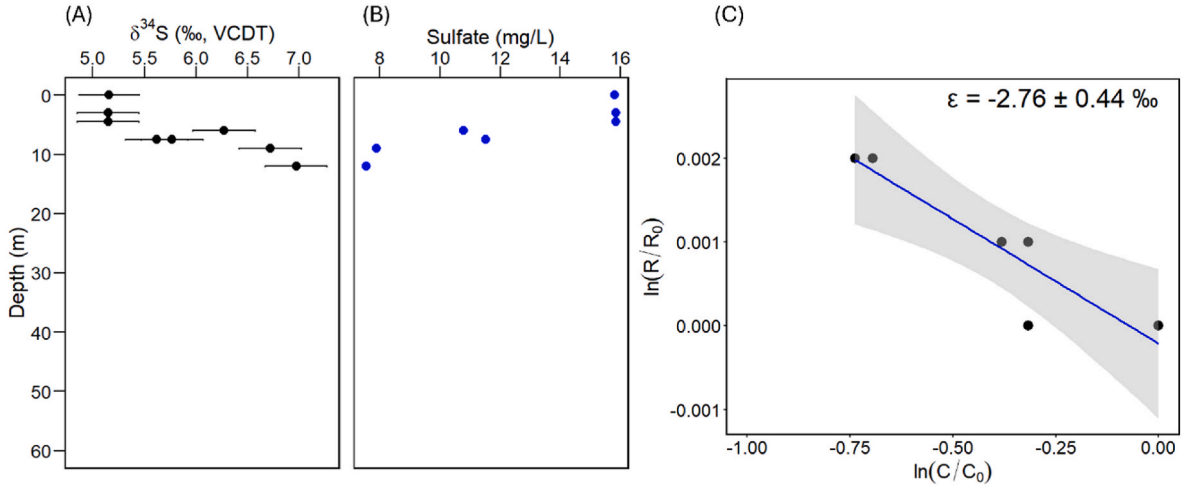


**Fig. 5.** $\delta^{34}S$-sulfate (A) and sulfate concentration (mg/L) (B) as a function of depth (sampling date: September 22, 2024). (C) Logarithmic plot according to the Rayleigh equation for sulfur isotopes.

**Table 1**
Concentrations of elements (ppm) determined by XRF in the sediment collected at 52 m in a mine level, as well as approximate weight (%).

| Element | Concentration (ppm) | ≈ wt (%) |
|---|---|---|
| Si | 90,088 | 9.0 |
| Ca | 78,130 | 7.8 |
| Fe | 65,876 | 6.6 |
| S | 43,943 | 4.4 |
| Mg | 34,509 | 3.4 |
| P | 20,403 | 2.0 |
| K | 17,744 | 1.8 |
| Al | 16,508 | 1.7 |
| Ti | 1768 | 0.2 |
| Cl | 313 | <0.1 |
| Mn | 237 | <0.1 |
| Zr | 233 | <0.1 |
| Ba | 200 | <0.1 |
| Sr | 198 | <0.1 |
| Cr | 182 | <0.1 |
| V | 106 | <0.1 |
| Zn | 39 | <0.1 |
| Rb | 25 | <0.1 |
| Bi | 16 | <0.1 |
| Nb | 8 | <0.1 |

at 36 m (2.3). Carbonate minerals were therefore the primary phases controlling the chemistry of the mine-impacted water in the open-pit lake.

### 3.8. Influence of depth and season on water chemistry

A PERMANOVA analysis showed that water chemistry was strongly influenced by depth ($R^2 = 0.68, p < 0.01$) and DO ($R^2 = 0.55, p < 0.01$), but not by season ($p > 0.05$). Depth groups (0 – 4 m, 5 – 15 m, >15 m) differed statistically significantly ($R^2 = 0.72$, $p < 0.001$) and DO also showed significant group differences ($R^2 = 0.60, p < 0.001$), consistent with the observed stratification. Spearman correlations revealed a strong negative relationship between sulfate concentration and $\delta^{34}S–SO_4$ ($\rho = -0.89$, $p < 0.001$). A redundancy analysis (RDA) was performed to examine the relationship between chemical variables (concentrations of dissolved elements and sulfate isotopes) and environmental variables (DO concentration, season and depth). The analysis showed that DO and depth explained most of the variance in the dataset (71% on axis 1), with a secondary effect on axis 2 (3%).

## 4. Discussion

### 4.1. Stratification of the water column

The temperature profile showed several distinct layers with stable conditions throughout the monitoring periods in 2023, 2024 and 2025. Multivariate statistical analyses (RDA and PERMANOVA) consistently showed that depth and DO were the dominant structuring factors of the water column, explaining most of the variability in water chemistry (depth: $R^2 = 0.68$; DO: $R^2 = 0.55$; axis 1 of RDA = 71% of variance) while seasonal effects were negligible, confirming a strong vertical stratification. This vertical stratification was comparable to that observed in meromictic lakes, such as the Pavin Lake in France (Olive and Boulègue, 2004; Omaly, 1968) or the pre-2010 Berkeley pit lake in the USA (Gammons and Icopini, 2020; Pellicori et al., 2005), that maintain a permanently stratified water column with an isolated monimolimnion that does not participate in seasonal mixing (Boehrer and Schultze, 2008; Wetzel, 2001). The epilimnion, a well-mixed surface layer, was relatively warm and oxygenated, and seasonal variations influenced the temperature. The presence of a thermocline at 5 m depth separated the epilimnion from the metalimnion, which corresponded to a thin transition layer (<2 m) where the temperature decreased rapidly with depth (Fig. 3A). The mixolimnion (including the epilimnion and metalimnion) had a relatively stable thickness of about 8 – 9 m during the sampling period. However, the vertical resolution of the measurements did not allow a clear distinction between the epilimnion and metalimnion. Finally, the monimolimnion was a colder, thermally stable layer located below the chemocline, characterized by permanently anoxic conditions with DO concentrations below detection limits (Fig. 3D). It can be subdivided into an upper zone just beneath the chemocline within the pit lake, and a lower zone corresponding to the working levels (>30 m) where concentrations of dissolved elements were higher due to the lack of dilution from surface inputs such as precipitation or snowmelt (Fig. 6). In meromictic lakes, the depths of the mixolimnion has been shown to vary with lake morphometry, with deeper and narrow basins exhibiting shallower mixolimnion, indicating that basin shape and maximum depth influence the stability of stratification (McGuire and Currie, 1993). In narrow and deep pit lakes, such as pit lakes at Cluff Lake (maximum depths of 28 and 90 m), seasonal mixing is restricted to the mixolimnion, allowing persistent chemical stratification to develop (Von Gunten et al., 2018). This is consistent with observations in other flooded pit lakes where morphometry and high relative depth strongly limit wind-driven mixing and promote persistent stratification (Castendyk and Eary, 2009; Geller et al., 2013). In contrast, in larger and shallower lakes, such as Crawford Lake, the mixolimnion reaches 15.5 m for a total depth of 24 m (McCarthy et al., 2023).

Water isotope values in the monimolimnion plot on the LMWL, whereas surface water samples clearly fall below this LMWL in 2024, especially during summer and autumn (Fig. 2A–C). This indicates that all water originates from the same source, which is the average meteoric recharge water for the area, but that surface water undergoes evaporation. The lighter isotopic value measured at the surface in spring, compared to other seasons, reflects a combination of inputs from isotopically lighter snowmelt and meteorological conditions that are less conducive to evaporation. Maximum change in isotope values at the surface reached about 1.5‰ for $\delta^{18}O$ (approximately 10‰ for $\delta^{2}H$). In comparison with other flooded mines, such as the Berkeley Pit (Butte, Montana), where surface waters have been estimated to undergo 10 – 25% evaporation (Gammons et al., 2006b; Pellicori et al., 2005), evaporation at the Blackburn Mine in 2024 appears substantially more limited (on the order of 2 – 3%; however, as the hydrological model required to accurately quantify evaporation was not developed for this site, this remains an estimate). The summers of 2023 and 2025 were particularly hot, with average maximum and minimum temperatures of 2.0 °C and 2.2 °C above normal, respectively, followed by an unusually warm September in both years and below-normal precipitation across several regions of Quebec (MELCCFP, 2023b, 2023a, 2025b, 2025a). As a result, the 1.5 m water level decline observed in 2025 likely represents the upper range of variability for the open pit lake, with similar patterns also observed in 2023 and 2024 (SI, Fig. S2).

In the Blackburn pit lake, the vertical isotopic gradient is largely controlled by stratification, the latter limit ting vertical mixing. As a result, $\delta^{18}O$ and $\delta^{2}H$ values in 2024 are either comparable to meteoric water signatures for deep water, or bear evidence of evaporation in the case of shallow points, with almost no values falling in between. These profiles are characteristic of meromictic lakes, with distinct isotopic signatures between the mixolimnion and the monimolimnion (Seebach et al., 2008; Vasil'chuk et al., 2018). A similar isotopic gradient has been observed in other open pit lakes, such as the Berkeley Pit, where density stratification and limited water circulation maintain a marked contrast between surface water affected by evaporation and deeper water that retain a meteoric signature (Gammons et al., 2006b; Pellicori et al., 2005).

Water isotopes values in 2025 fall within the same range as those observed in 2024, except within a depth interval between 30 and 42 m, corresponding to the bottom of the open pit lake and the working level, where unexpectedly enriched values are observed, reaching up to −6‰ for $\delta^{18}O$ at 36.6 m (samples collected on June 8, 2025, Fig. 2E and F). As

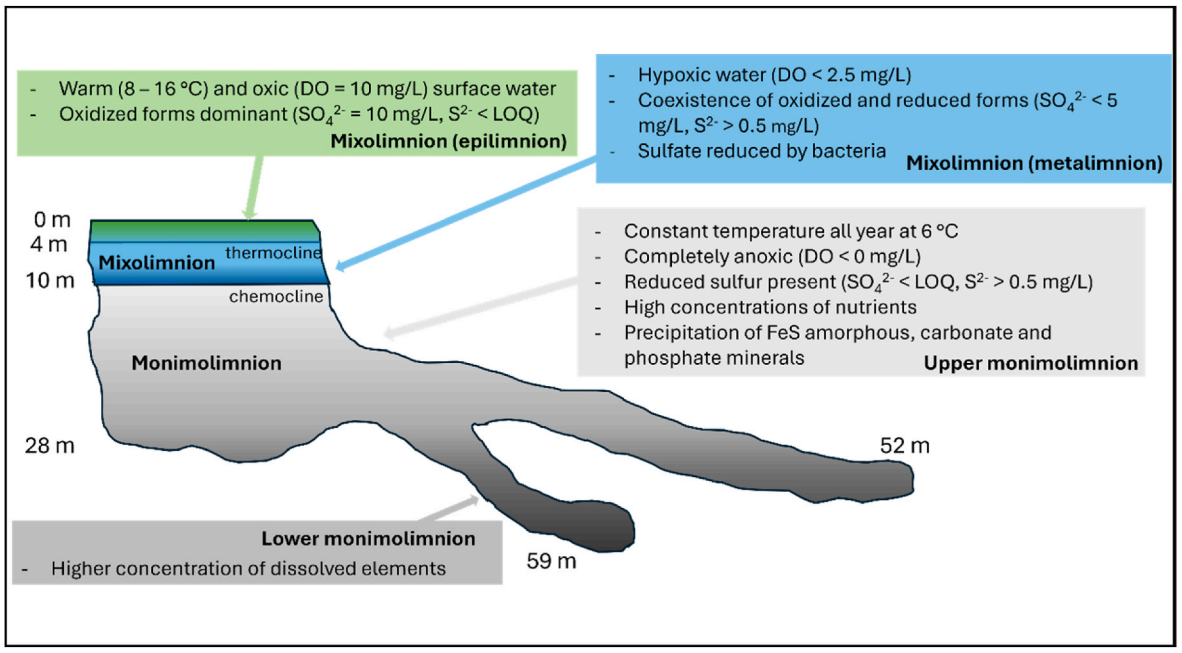


**Fig. 6.** Stratification of mine water and the specific characteristics of each layer.

several samples from adjacent depths exhibit similarly enriched values, an issue related to sample handling can be ruled out. This shift in isotopic values could indicate lateral inflow from a distinct groundwater source rather than vertical mixing, as the $\delta^{18}O$ and $\delta^{2}H$ profiles differ from those expected after mixing: vertical mixing tends to homogenize isotopic values throughout the water column, whereas the observed enrichment is localized (Gibson et al., 2016; Harning et al., 2024; Kankaala et al., 2023). However, the chemical composition of these samples is very similar to that of adjacent samples, which weakens the hypothesis of lateral groundwater inflow. Furthermore, the high isotopic values are inconsistent with those expected for modern meteoric water in the area.

### 4.2. *Water chemistry and governing processes*

#### 4.2.1. *Evolution of water chemistry*

Much lower concentrations of trace metals and sulfate were measured in this non-metallic mica and phosphate mine lake compared to metal- and coal-mine open pit lakes, although not all trace elements were included in the measurements. The latter pit lake typically exhibit high concentrations of pyrite and other sulfides, along with very low pH, as commonly observed at acid-mine drainage (AMD) sites such as the Berkley pit in the USA (Pellicori et al., 2005) or La Cueva de la Mora in Spain (Sánchez-España et al., 2009). As a result, the site shows no indication of contamination that would pose a relevant threat to the surrounding environment or necessitate mitigation or remediation (SI, Table S3).

Private wells exhibited EC values comparable to those observed within the pit lake (Fig. 3B and SI, Tables S5 and S6). In the flooded open pit, the upper layers (0 – 15 m) showed lower TDS concentrations and EC values than the pit lake (SI, Table S6), indicating dilution by precipitation and snowmelt. A regional bedrock well sampled for the PACES-OUT program in 2013 (ID: 21839, Code: SIH_2007-150-73500039, PACES-OUT (Comeau et al., 2013; MELCCFP, 2013)) showed similar TDS concentrations (494 mg/L) and EC values (760 µS/cm) to those observed in the mine levels and private wells in this study. Physicochemical analyses showed that mine water (open pit lake and working levels) and private wells, that were drilled in the bedrock (80 – 92 m deep, estimations provided by the well owners via personal communications), exhibited a hydrogen carbonate type water typical of local bedrock aquifers, reflecting the nature of the regional geological formations, which are metamorphosed skarns and calc-silicates (Comeau et al., 2013) (SI, Fig. S3).

Relatively high dissolved fluoride concentrations were detected in the mine water and the well water, at concentrations up to 1.7 mg/L (SI, Fig. S5E and Table S3). At a broader regional scale, several wells used for drinking water supply had fluoride concentrations above the maximum acceptable concentration of 1.5 mg/L (Comeau et al., 2013; Règlement sur la qualité de l'eau potable., 2025). These exceedances are consistent with the presence of fluorite in the surrounding rocks, which has a much higher solubility than fluorapatite in natural waters (see Section 2.1.). At the regional scale, fluoride exceedances were likely associated with cation exchange between $Ca^{2+}$ and $Na^{+}$, which enhanced fluorite dissolution through the removal of calcium by adsorption. Consistent with both the presence of fluorapatite in the host lithology and its accumulation in the anoxic layer, phosphate concentrations were relatively high in the mine water, representing a key nutrient in the water column (see Section 4.3.).

$\delta^{34}S$–$SO_4$ values, ranging from 5.2 to 7.0‰, suggest that sulfate is of lithogenic origin (André et al., 2002; Banks and Boyce, 2023; Dold and Spangenberg, 2005). Sulfate concentrations were low and consistent with reducing conditions in the water column, where PHREEQC simulations indicated sulfide stability (as FeS and pyrite, see Section 4.2.3.). This suggests that sulfur is predominantly present in reduced mineral phases, limiting sulfate accumulation in the system (Meinert, 1992; Vernon, 2004). Sulfate concentrations remained low compared to those reported in ore pit lakes or metal mines affected by acid mine drainage, where (di-)sulfide oxidation can lead to extreme sulfate concentrations (Castendyk and Eary, 2009; Gammons et al., 2009; Geller et al., 2013; Roesler et al., 2007; Sánchez-España et al., 2009).

#### 4.2.2. *Profiles of other parameters along the water column*

Dissolved oxygen profiles showed strong stratification of the water column: surface water was oxic, but oxygen concentrations declined sharply, reaching anoxic conditions at 5 m year-round, with the water remaining completely anoxic below this depth (Fig. 3D). This vertical structure reflects that DO is a key driver of chemical differentiation along the water column, as shown by statistical analyses. The absence of

nitrate and nitrite in mine water, even at the surface, combined with the presence of nitrate in surrounding oxygenated groundwater (SI, Table S5), suggests that any nitrate entering the water column is rapidly consumed by denitrification. Despite relatively high ammonium concentrations (see Section 4.3.), the absence of oxygen in the water column prevents nitrification. No denitrifying microorganisms were identified in the water column (Lhoste et al., 2026). Concentration profiles of dissolved manganese and iron indicate reduction of both manganese and iron oxides below 5 m in the open pit lake and in the working levels (Fig. 3E and F). Concentrations remained below 0.3 mg/L for Mn and 0.15 mg/L for Fe, likely due to precipitation of Fe- and Mn- bearing minerals (see Section 4.2.3.).

The enrichment in heavier sulfate isotopes with depth, from $\delta^{34}S–SO_4$ = 5.2‰ to = 7‰, in combination with decreasing sulfate concentrations (Fig. 5), indicates that microbial sulfate reduction by sulfate-reducing bacteria (SRB) occurs below 5 m (Canfield, 2001; IAEA, 2008; Jørgensen and Kasten, 2006). Spearman correlations also revealed a strong negative relationship between sulfate concentration and $\delta^{34}S–SO_4$ ($p = -0.89$; $p < 0.001$), consistent with isotopic fractionation during sulfate reduction. In contrast, groundwater, which showed higher sulfate concentrations and was generally oxygenated, had $\delta^{34}S–SO_4$ values < 5.1‰, indicating that sulfate-reducing bacteria (SRB) were not present (SI, Table S5 and Fig. S6). Surprisingly, $\delta^{18}O–SO_4$ did not show the same trend as $\delta^{34}S–SO_4$, as would be expected for SRB metabolism (Bertran et al., 2020), but instead varied randomly with depth (Fig. S6). As the oxygen of dissolved sulfate and water can rapidly exchange at pH < 2 (Bradley et al., 2016; Canfield, 2001; Kaplan and Rittenberg, 1964), a sample preparation artefact cannot be excluded, although pH was maintained above 4. Oxygen isotope data are therefore not discussed further. The occurrence of sulfate reduction is further supported by another study conducted in the mine, which confirmed the presence of SRB between 6 and 12 m (Lhoste et al., 2026).

Previous studies have shown that the magnitude of sulfur isotope fractionation can be influenced by several factors, including sulfate availability and organic carbon supply (Bradley et al., 2016; Canfield, 2001). The enrichment factor of −2.4‰ determined here is below the typical range expected for hydrological settings, generally between −10 and −20‰ (Aelion et al., 2009). Although dissolved organic carbon has not been measured in this study, it is likely that SRB are limited by sulfate availability, which would constrain isotope fractionation and explain the relatively low enrichment factor. In AMD contexts, such as La Cueva de la Mora, the opposite occurs: abundant sulfate and low organic carbon reduce the activity of SRB due to the limited availability of electron donors for sulfide production (Liu et al., 2024), leading to pronounced isotope fractionation.

Reduced sulfur species, such as $H_2S$ originating from sulfate reduction, can serve as an energy source for sulfur-oxidizing bacteria (SOB) such as *Sulfuricurvum*, which were abundant at 52 m depth in the working levels (Lhoste et al., 2026). Additionally, a phototrophic purple sulfur bacterium (PSB), *Thiodictyon*, which uses $H_2S$ as an electron donor, has been identified in the 6 – 12 m zone, highlighting an active sulfur cycle in this layer of the open pit lake (Lhoste et al., 2026). PSB are often found at the chemocline of meromictic lakes (Di Nezio et al., 2021; Meyer et al., 2011).

#### 4.2.3. Controls of water chemistry

X-ray fluorescence analysis of the sediments revealed high concentrations of Fe and S (approximately 6.6 wt % and 4.4 wt %, respectively, Table 1). PHREEQC simulations showed that mackinawite (FeS) had a SI > 1 at 36 m, while pyrite ($FeS_2$) was several orders of magnitude supersatured at 36 m, indicating likely precipitation of these phases. These results, in combination with the observed black color, indicate the presence of metal sulfides in the sediments, which is consistent with anoxic conditions and depletion of electron acceptors observed in the open pit lake and in working levels, and could also explain the low concentration of dissolved sulfur in the water column (Thiel et al., 2019), a scenario already observed in the Butte open pit lake in Montana (Roesler et al., 2007). In sulfidic water, the concentrations of dissolved $Fe^{2+}$ and $S^{2-}$ are primarily controlled by the saturation of amorphous FeS or mackinawite rather than by pyrite itself (Hunger and Benning, 2007; Rickard, 1997). Amorphous FeS and mackinawite are subsequently converted to pyrite under favorable conditions, consistent with the results of PHREEQC simulations. Similar observations have been reported in the Butte mine, where sulfide precipitation occurs in anoxic zones, producing mineral assemblages that include both metastable FeS phases and pyrite, reflecting progressive mineral transformations under anoxic conditions (Gammons et al., 2009; Roesler et al., 2007). The Fe/S molar ratio of the sediments is 0.86, which is much closer to that of mackinawite (1) than to that of pyrite (1.5). This result suggests that the sediments are relatively iron-rich compared to sulfur, and that (i) they likely contain poorly crystalline or early-stage iron sulfides, or (ii) other Fe-bearing minerals, such as siderite ($FeCO_3$), may also precipitate. Siderite was slightly undersaturated at 36 m (SI = −0.7), consistent with the presence of reduced sulfur species, which limit Fe availability, despite anoxic conditions and high dissolved hydrogenocarbonate concentrations.

The high concentrations of Ca and Mg revealed by XRF analyses (7.8 wt % and 3.4 wt %, respectively, Table 1), combined with PHREEQC simulations showing calcite ($CaCO_3$) and rhodochrosite ($MnCO_3$) close to equilibrium at 36 m (SI of 0.2 and −0.1, respectively), indicate the presence of carbonate minerals in the sediments. This observation is consistent with the increase of alkalinity with depth following microbial activity (Fig. 3I), which promoted carbonate precipitation in the open pit lakes and in the working levels.

Hydroxyapatite ($Ca_5(PO_4)_3(OH)$) was supersaturated at 36 m (SI = 2.3), which is consistent with the relatively high amount of P measured in the sediments (2.0 wt %), as well as the increase in phosphate concentrations with depth (Fig. S5F). It is also very likely that native fluorapatite was present in the sediments; however, its occurrence cannot be confirmed by XRF measurements due to the inability to detect fluorine. Finally, the amount of Si and K measured in the sediments suggest the presence of silicate minerals, such as quartz and orthoclase, originating from the surrounding rocks. Trace element indicators also suggest the occurrence of zircon and Ti-bearing minerals, which is consistent with the minerals known to occur at the site (Sabina, 1987).

To summarize, concentrations of ferrous iron and reduced sulfur species in the water column are very likely controlled by the precipitation of amorphous FeS, while the precipitation of carbonate minerals such as calcite controls calcium and hydrogenocarbonate concentrations, rhodochrosite controls dissolved manganese, and phosphate concentrations are regulated by the precipitation of phosphate minerals such as hydroxyapatite. These controls have been documented in flooded mine and meromictic environments, where strong gradients in oxygen concentrations and electron acceptor distribution promote the sequential precipitation of sulfides, carbonates and phosphate minerals (Gammons et al., 2006a; Thiel et al., 2019).

### 4.3. Trophic status and nutrients in the water column

Vertical profiles revealed a meso-eutrophic photic zone (0 – 4 m; TSI 56 – 60; Secchi depth = 5 m), indicating moderate surface productivity (Carlson, 1977; OECD, 1982), with phytoplankton biomass ranging from 8 to 25 µg/L Chl *a*. Below the thermocline, in the monimolimnion, nutrient concentrations were substantially higher than at the surface (TP up to 124 µg/L; TN 0.93 mg/L; Chl *a*n up to 55 µg/L; TSI >80), reflecting the accumulation of nutrients under anoxic conditions due to the stratification of water that limited vertical mixing (Fig. 4 and SI, Fig. S5F). This internal nutrient enrichment of anoxic, deeper water is well documented in stratified eutrophic lakes (Nürnberg, 1984; Søndergaard et al., 2003), and similar enrichment patterns have been observed in other meromictic lakes. In Lake Lubińskie (TSI = 61),

vertical nutrient distributions, low visibility (2 m), TP (130 μg/L) and TN (3.8 mg/L) profiles indicate productivity restricted to certain layers (Zieliński et al., 2019). The vertical distribution of ammonium and phosphate is primarily controlled by depth and DO, as also indicated by multivariate analyses (see Section 3.8.). In the Blackburn pit lake, phosphorus and ammonium accumulation below the thermocline confirms that density, thermal stratification and internal processes regulate nutrient distribution, while the photic zone remains meso-eutrophic, reflecting biological dynamics and external inputs rather than vertical mixing.

The absence of nitrate and nitrite in the monimolimnion, combined with high $NH_4^+$ concentrations (up to 1.5 mg/L below 20 m, Fig. 4C), suggests active ammonification and/or accumulation of ammonium from organic matter in the sediments and in the anoxic water, while the lack of oxygen limits nitrification. The detection of an ammonia-oxidizing nanoarchaeon (strain designation: GW2011) in the Blackburn mine highlights the possible role of ammonium as a key ecological driver (Lhoste et al., 2026). However, since ammonium oxidation requires oxygen, this microbial activity is most likely confined to a suboxic zone, rather than in the strictly anoxic monimolimnion. In contrast, in the mixolimnion, the shallow, oxygenated photic layer promotes rapid biological uptake of nitrogen and phosphorus, contributing to the relatively low dissolved nitrogen concentrations near the surface. These observations are consistent with those reported in other stratified pit lakes, where microbial mineralization in deep water and redox-controlled nutrient transformations along the water column induced similar vertical redox and nutrient gradients (Castendyk and Eary, 2009; Geller et al., 2013; Wetzel, 2001).

The observed accumulation of Chl *a* below the photic zone has been often described in stratified waters and may result from two non-exclusive mechanisms. First, accumulation of pigments from dead or slowly degraded phytoplankton as well as detritus can lead to elevated Chl *a* concentrations without indicating active photosynthesis (Cullen, 2015). Second, the presence of mixotrophic eukaryotes at these depths, which combine photosynthesis with bacterivory, may contribute to the retention of Chl *a* in deeper water (Lhoste et al., 2026; Stoecker et al., 2017).

### 4.4. Persistence of meromixis

The Blackburn open pit lake exhibits several characteristics typical of meromictic lakes: (i) a strong and apparently stable stratification (supported by RDA and PERMANOVA analyses identifying depth and DO as the main structuring factors with negligible seasonal effects), (ii) a pronounced gradient in oxygen and electron acceptor availability between layers, with an oxygenated mixolimnion and an anoxic monimolimnion characterized by an enrichment in nitrogen and phosphorus, and (iii) the presence of microorganisms typical of such environments (Lhoste et al., 2026).

The Blackurn open pit lake is relatively deep and narrow, with an approximately 10 m high wall surrounding the pit lake (Fig. 1D). This morphology is expected to reduce wind exposure and limit mechanical mixing of the water column. This is consistent with the concept of relative depth, where pit lakes with high depth-to-surface area ratios experience reduced wind-driven mixing and more persistent stratification compared to natural lakes (Castendyk and Eary, 2009; Geller et al., 2013). Similar cases include Lake Pavin (a natural volcanic lake) and Iron Mountain (an open-pit lake), both of which are meromictic lakes (Bond et al., 2000; Olive and Boulègue, 2004). During the sampling period in 2024 and 2025 (from May to October), the water column of the Blackburn pit lake exhibited stable stratification, with a denser, slightly more mineralized lower layer ($\rho = 1000.19$ kg/m$^3$ at 43 m) underlying less mineralized surface water in the open pit lake ($\rho = 999.65$ kg/m$^3$ at 1.5 m, Table S6). While the amplitude of the density gradient was smaller than in some meromictic AMD environments, such as La Cueva de la Mora (Sánchez-España et al., 2009), similar seasonal stability and solute-driven density stratification have been observed in low-mineralization lakes, where moderate but persistent density differences were sufficient to limit vertical mixing (Olive and Boulègue, 2004).

This weak density gradient, combined with the regional climate, suggests the potential for occasional lake overturn. Temperatures measured in the mixolimnion ranged from 8 °C (late October 2024) to 16 °C (summer 2024, Fig. 3A). Given the local climate (SI, Fig. S1), the temperature of the mixolimnion could reach 4 °C in early spring or late autumn, when the lake is free of ice but outside of the sampling period, hence attaining the maximum density and leading to a complete or partial lake overturn. While partial mixing of the mixolimnion could occur without disturbing the monimolimnion (Boehrer and Schultze, 2008), the thin mixolimnion makes this unlikely. The sole hint of partial or complete overturn is provided by some EC measurements in spring, which reached nearly 400 μS/cm, whereas values later in the sampling season were around 300 μS/cm or lower (Fig. 3B). While convective cells have been observed in some flooded mines under specific thermal and density gradients (Mugova and Wolkersdorfer, 2022), the small density differences and limited temperature variations observed in the Blackburn pit lake suggest that such processes are unlikely to occur.

## 5. Conclusion

The study of the flooded Blackburn open pit revealed a well-stratified, meromictic water column, characterized by an oxygenated 8 – 9 m thick mixolimnion and a thermocline located at around 5 m, overlying a stable, anoxic, and more mineralized monimolimnion below 11 – 12 m, separated by a 1 – 1.5 m thick chemocline. Depth and dissolved oxygen strongly controlled the chemistry of the water column, while TDS concentrations and density differences, although small, were sufficient to maintain seasonal thermal and density stratification. Seasonal processes such as snowmelt or ice cover may promote partial vertical mixing; however, there is limited evidence that such mixing occurred during the sampling period. Stable stratification led to accumulation of nutrients in the monimolimnion, emphasizing the role of internal recycling in shaping nutrient distribution. Sulfate reduction was evidenced in the upper part of the monimolimnion, and the formation of metal sulfides, as well as carbonate precipitation, represented key controls on water chemistry.

Given the lack of studies on flooded abandoned apatite and/or mica mines in this region, the Blackburn open pit lake represents a useful model system that may be representative of similar artificial aquatic environments. The insights gained from this study could inform the monitoring, prioritization, and management of abandoned, flooded non-metallic mica and apatite mines in Quebec and across Canada.

## Funding

This research was supported by a NOVA Natural Sciences and Engineering Research Council (NSERC) and Fonds de Recherche-Nature et Technologie (FRQNT) grant awarded to C.S.L., V.*P. and* D.J [2023-NOVA-314112], as well as a NSERC discovery grant awarded to VP [RGPIN-2021-03309]. This research, conducted at Geotop, also received funding from the Fonds de recherche du Québec (https://doi.org/10.69777/341269. Cliquez ou appuyez si vous faites confiance à ce lien.">https://doi.org/10.69777/341269).

## CRediT authorship contribution statement

**Élisa Pastier:** Conceptualization, Formal analysis, Investigation, Methodology, Visualization, Writing – original draft. **Élise Lhoste:** Investigation, Writing – review & editing. **David Jaclin:** Funding acquisition, Writing – review & editing. **Cassandre Sara Lazar:** Conceptualization, Funding acquisition, Project administration,

Supervision, Writing – review & editing. **Violaine Ponsin:** Conceptualization, Funding acquisition, Methodology, Project administration, Supervision, Writing – review & editing.

## Declaration of competing interest

The authors declare that they have no known competing financial interests or personal relationships that could have appeared to influence the work reported in this paper.

## Acknowledgments

The authors would like to thank the diving team of PTO Exploration and Minex Project members: Guy Allard, David Caissy, Kevin Brown, Alain Delisle, Pierre Groulx, Bertrand Favreau, Steve Duplessis, Caroline Joanis, Ariane Monfils, Yvan Dion for their invaluable help in this project. The authors would also like to thank Gwénael Chamoulaud, Katherine Velghe and Jean-François Hélie for assistance with the measurements, as well as Matias Levesque-Vargas, Marilys Mercure-Nadeau and Donovan Despaud for their help during field work. We would like to thank the two anonymous reviewers for their constructive comments, which substantially improved the quality of this manuscript.

## Appendix A. Supplementary data

Supplementary data to this article can be found online at https://doi.org/10.1016/j.apgeochem.2026.106962.

## Data availability

Data will be made available on request.

## References

Aelion, C., Hohener, P., Hunkeler, D., Aravena, R., 2009. Envrionnemental Isotopes in Biodegradation and Bioremediation. CRC Press.

André, L., Franceschi, M., Pouchan, P., Atteia, O., 2002. Origine et évolution du soufre au sein de l'aquifère des Sables infra-molassiques du Bassin aquitain. C. R. Geosci. 334 (10), 749–756. https://doi.org/10.1016/S1631-0713(02)01814-X.

Association Minière du Québec, 2022. Types de mines. Association Minière du Québec. https://amq-inc.com/types-de-mines/.

Atanacković, N., Dragišić, V., Stojković, J., Papić, P., Živanović, V., 2013. Hydrochemical characteristics of mine waters from abandoned mining sites in Serbia and their impact on surface water quality. Environ. Sci. Pollut. Control Ser. 20 (11), 7615–7626. https://doi.org/10.1007/s11356-013-1959-4.

Banks, D., Boyce, A.J., 2023. Dissolved sulfate $\delta^{34}$ S and the origin of sulfate in coal mine waters; NE England. Q. J. Eng. Geol. Hydrogeol. 56 (2), qjegh2022–q2106. https://doi.org/10.1144/qjegh2022-106.

Bertran, E., Waldeck, A., Wing, B.A., Halevy, I., Leavitt, W.D., Bradley, A.S., Johnston, D. T., 2020. Oxygen isotope effects during microbial sulfate reduction: applications to sediment cell abundances. ISME J. 14 (6), 1508–1519. https://doi.org/10.1038/s41396-020-0618-2.

Boehrer, B., Schultze, M., 2008. Stratification of lakes. Rev. Geophys. 46 (2). https://doi.org/10.1029/2006RG000210.

Bond, P.L., Druschel, G.K., Banfield, J.F., 2000. Comparison of acid mine drainage microbial communities in physically and geochemically distinct ecosystems. Appl. Environ. Microbiol. 66 (11), 4962–4971. https://doi.org/10.1128/AEM.66.11.4962-4971.2000.

Bradley, A.S., Leavitt, W.D., Schmidt, M., Knoll, A.H., Girguis, P.R., Johnston, D.T., 2016. Patterns of sulfur isotope fractionation during microbial sulfate reduction. Geobiology 14 (1), 91–101. https://doi.org/10.1111/gbi.12149.

Bridgewater, L.L., Baird, R.B., Eaton, A.D., Rice, E.W., American Public Health Association, American Water Works Association, 2017. Water environment Federation. In: Standard Methods for the Examination of Water and Wastewater, 23rd edition. American Public Health Association.

Canfield, D.E., 2001. Isotope fractionation by natural populations of sulfate-reducing bacteria. Geochem. Cosmochim. Acta 65 (7), 1117–1124. https://doi.org/10.1016/S0016-7037(00)00584-6.

Carlson, R.E., 1977. A trophic state index for lakes1. Limnol. Oceanogr. 22 (2), 361–369. https://doi.org/10.4319/lo.1977.22.2.0361.

Castendyk, D.N., Eary, L.E. (Eds.), 2009. Mine Pit Lakes: Characteristics, Predictive Modeling, and Sustainability. Society for Mining, Metallurgy & Exploration, vol. 3. Inc.

Centre d'expertise en analyse environnementale du Québec (CEAEQ), 2023. Détermination des sulfures: méthode colorimétrique avec le chlorure ferrique et l'oxalate de N,N-diméthyle-p-phénylènediamine. Ministère de l'Environnement du Québec. https://www.ceaeq.gouv.qc.ca/methodes/pdf/methode-analyse-300-sulfures.pdf.

Chlahbi, S., 2024. *Upstream geomineralurgical characterization of a sedimentary phosphate deposit for mine waste sustainable management and valorization purposes* [Université du Québec en Abitibi-Témiscamingue]. https://depositum.uqat.ca/id/eprint/1661/.

Clark, I., Fritz, P., 1997. Environnemental Isotopes in the Hydrological Cycle. CRC Press).

Comeau, G., Talbot Poulin, M., Tremblay, Y., Ayotte, S., Molson, J., Lemieux, J., Montcoudiol, N., Therrien, R., Fortier, R., Therrien, P., Fabien-Ouellet, G., 2013. Projet d'Acquisition des connaissances des Eaux Souterraines en Outaouais (PACES-OUT). Université de Laval 311 [Rapport final].

Cullen, J.J., 2015. Subsurface chlorophyll maximum layers: enduring enigma or mystery solved? Ann. Rev. Mar. Sci 7 (1), 207–239. https://doi.org/10.1146/annurev-marine-010213-135111.

Des Mines Et Des Hommes: Histoire De L'Industrie Minérale Québécoise Des Origines À Aujourd'Hui (Édition Revue Et Augmentée), 2012. Publications du, Québec.

Di Nezio, F., Beney, C., Roman, S., Danza, F., Buetti-Dinh, A., Tonolla, M., Storelli, N., 2021. Anoxygenic photo- and chemo-synthesis of phototrophic sulfur bacteria from an alpine meromictic lake. FEMS (Fed. Eur. Microbiol. Soc.) Microbiol. Ecol. 97 (3). https://doi.org/10.1093/femsec/fiab010 fiab010.

Dold, B., Spangenberg, J.E., 2005. Sulfur speciation and stable isotope trends of water-soluble sulfates in mine tailings profiles. Environ. Sci. Technol. 39 (15), 5650–5656. https://doi.org/10.1021/es040093a.

Fuchs, A., Casper, P., Lewandowski, J., 2022. Dynamics of greenhouse gases ($CH_4$ and $CO_2$) in Meromictic Lake Burgsee, Germany. J. Geophys. Res. Biogeosci. 127 (8), e2021JG006661. https://doi.org/10.1029/2021JG006661.

Gammons, C.H., Henne, W., Poulson, S.R., Parker, S.R., Johnston, T.B., Dore, J.E., Boyd, E.S., 2014. Stable isotopes track biogeochemical processes under seasonal ice cover in a shallow, productive lake. Biogeochemistry 120 (1–3), 359–379. https://doi.org/10.1007/s10533-014-0005-z.

Gammons, C.H., Metesh, J.J., Snyder, D.M., 2006a. A Survey of the geochemistry of flooded mine shaft water in Butte, Montana. Mine Water Environ. 25 (2), 100–107. https://doi.org/10.1007/s10230-006-0117-3.

Gammons, C.H., Poulson, S.R., Pellicori, D.A., Reed, P.J., Roesler, A.J., Petrescu, E.M., 2006b. The hydrogen and oxygen isotopic composition of precipitation, evaporated mine water, and river water in Montana, USA. J. Hydrol. 328 (1–2), 319–330. https://doi.org/10.1016/j.jhydrol.2005.12.005.

Gammons, C.H., Snyder, D.M., Poulson, S.R., Petritz, K., 2009. Geochemistry and stable isotopes of the flooded underground mine workings of Butte, Montana. Econ. Geol. 104 (8), 1213–1234. https://doi.org/10.2113/gsecongeo.104.8.1213.

Gammons, C.H., Icopini, G.A., 2020. Improvements to the water quality of the acidic Berkeley Pit Lake due to copper recovery and sludge disposal. Mine Water Environ. 39 (3), 427–439. https://doi.org/10.1007/s10230-019-00648-8.

Gatineau Valley Historical Society (GVHS), 1998. Stanislas Franchot and his Buckingham Mines.

Geller, W., Schultze, M., Kleinmann, R., Wolkersdorfer, C. (Eds.), 2013. Acidic Pit Lakes: the Legacy of Coal and Metal Surface Mines. Springer Berlin Heidelberg. https://doi.org/10.1007/978-3-642-29384-9.

Gibson, J.J., Birks, S.J., Yi, Y., 2016. Stable isotope mass balance of lakes: a contemporary perspective. Quat. Sci. Rev. 131, 316–328. https://doi.org/10.1016/j.quascirev.2015.04.013.

Government of Canada, 2023. Rapport de données quotidiennes pour février 2026 – station Ottawa CDA (6105976). Climat – Météo-Canada. https://climate.weather.gc.ca/climate_data/daily_data_e.html?hlyRange=%7C&dlyRange=1889-11-01%7C2026-02-02&mlyRange=1889-01-01%7C2006-12-01&climate_id=6105976&Prov=ON&urlExtension=_f.html&searchType=stnName&optLimit=yearRange&StartYear=1840&EndYear=2026&selRowPerPage=25&Line=7&searchMethod=contains&Month=2&Day=11&txtStationName=Ottawa&timeframe=2&Year=2026.

Government of Canada, Natural Resources Canada, 2026. Orphaned and Abandoned Mines in Canada. Government of Canada. Mines Canada. https://www.minescanada.ca/en/orphaned-and-abandoned-mines.

Harning, D.J., Raberg, J.H., McFarlin, J.M., Axford, Y., Florian, C.R., Ólafsdóttir, K.B., Kopf, S., Sepúlveda, J., Miller, G.H., Geirsdóttir, Á., 2024. Spatiotemporal variation of modern lake, stream, and soil water isotopes in Iceland. Hydrol. Earth Syst. Sci. 28 (18), 4275–4293. https://doi.org/10.5194/hess-28-4275-2024.

Hunger, S., Benning, L.G., 2007. Greigite: a true intermediate on the polysulfide pathway to pyrite. Geochem. Trans. 8 (1), 1. https://doi.org/10.1186/1467-4866-8-1.

Hunsinger, G.B., Tipple, C.A., Stern, L.A., 2013. Gaseous byproducts from high-temperature thermal conversion elemental analysis of nitrogen- and sulfur-bearing compounds with considerations for $\delta^2$ H and $\delta^{18}$ O analyses. Rapid Commun. Mass Spectrom. 27 (14), 1649–1659. https://doi.org/10.1002/rcm.6608.

IAEA (International Atomic Energy Agency), 2008. *Isotopes de l'environnement dans le cycle hydrologique* (Collection Cours de Formation N° 32F). https://wwwpub.iaea.org/mtcd/publications/pdf/tcs-32_fr_web.pdf.

Jørgensen, B.B., Kasten, S., 2006. Sulfur cycling and methane oxidation. In: Schulz, H.D., Zabel, M. (Eds.), Marine Geochemistry. Springer-Berlin, pp. 271–309. https://doi.org/10.1007/3-540-32144-6_8.

Kankaala, P., Sonninen, E., Einola, E., Huotari, J., Huttula, T., Mäkelä, S., Ojala, A., Rask, M., Tulonen, T., Arvola, L., 2023. Temporal and lake-specific variations in oxygen and hydrogen stable isotopes in a boreal lake-chain during two hydrologically differing years. Inland Waters 13 (3), 362–373. https://doi.org/10.1080/20442041.2023.2255118.

Kaplan, I.R., Rittenberg, S.C., 1964. Microbiological fractionation of sulphur isotopes. J. Gen. Microbiol. 34 (2), 195–212. https://doi.org/10.1099/00221287-34-2-195.

Keshri, J., Mankazana, B.B.J., Momba, M.N.B., 2015. Profile of bacterial communities in South African mine-water samples using Illumina next-generation sequencing

platform. Appl. Microbiol. Biotechnol. 99 (7), 3233–3242. https://doi.org/10.1007/s00253-014-6213-6.
Le Echo de la Tuque, 2022. Mine de mica: accord entre Wemotaci et Imerys Canada. Le Echo de la Tuque. https://www.lechodelatuque.com/actualites/mine-de-mica-accord-entre-wemotaci-et-imerys-canada/.
Lhoste, E., Comte, F., Brown, K., Delisle, A., Jaclin, D., Ponsin, V., Rosabal, M., Lazar, C. S., 2023. Bacterial, archaeal, and eukaryote diversity in planktonic and sessile communities inside an abandoned and flooded iron mine (Quebec, Canada). Appl. Microbiol. 3 (1), 45–63. https://doi.org/10.3390/applmicrobiol3010004.
Lhoste, E., Jaclin, D., Ponsin, V., Rosabal, M., Sara Lazar, C., 2026. Seasons and vertical dynamics influence community composition in a flooded and abandoned mica mine. FEMS (Fed. Eur. Microbiol. Soc.) Microbiol. Ecol. 102 (2), fiaf131. https://doi.org/10.1093/femsec/fiaf131.
Liu, Y., Macalady, J.L., Sánchez-España, J., Burgos, W.D., 2024. Enrichment of acid-tolerant sulfide-producing microbes from an acidic pit lake. Front. Microbiol. 15, 1475137. https://doi.org/10.3389/fmicb.2024.1475137.
Matheson, N., 1974. Modified methylene blue method for the micro determination of hydrogen sulphide. The Analyst 99 (1182), X033. https://doi.org/10.1039/an97499fx033.
McCarthy, F.M., Patterson, R.T., Head, M.J., Riddick, N.L., Cumming, B.F., Hamilton, P. B., Pisaric, M.F., Gushulak, A.C., Leavitt, P.R., Lafond, K.M., Llew-Williams, B., Marshall, M., Heyde, A., Pilkington, P.M., Moraal, J., Boyce, J.I., Nasser, N.A., Walsh, C., Garvie, M., et al., 2023. The varved succession of Crawford Lake, Milton, Ontario, Canada as a candidate Global boundary Stratotype Section and Point for the Anthropocene series. Anthropocene Rev. 10 (1), 146–176. https://doi.org/10.1177/20530196221149281.
McDougall, T.J., Barker, P.M., 2011. Getting Started with TEOS-10 and the Gibbs Seawater (GSW) Oceanographic Toolbox. Version 3.0 (Version 3). SCOR/IAPSO WG127.
McGuire, S., Currie, D.J., 1993. Factors related to the variation in mixing depth among meromictic Lakes. Can. J. Fish. Aquat. Sci. 50 (6), 1338–1342. https://doi.org/10.1139/f93-152.
Meinert, L.D., 1992. Skarns and skarn deposits. Geosci. Can. 19 (4), 145–162. https://doi.org/10.12789/gs.v19i4.3773.
MELCCFP, 2023a. *Été 2023: une chaleur record au nord fait de cet été le plus chaud des archives au Québec* [Gouvernement du Québec]. https://www.environnement.gouv.qc.ca/climat/Faits-saillants/2023/ete.htm.
MELCCFP, 2023b. *Septembre 2023: le mois de septembre le plus chaud des archives et le plus sec depuis 1950 au Québec* [Gouvernement du Québec]. https://www.environnement.gouv.qc.ca/climat/Faits-saillants/2023/septembre.htm.
MELCCFP, 2025a. Août 2025: Une Intense Canicule Et Des Minimums De Pluie Records À Plusieurs Endroits Au Sud De La Province [Gouvernement du Québec]. https://www.environnement.gouv.qc.ca/climat/Faits-saillants/2025/aout.htm.
MELCCFP, 2025b. Septembre 2025: un minimum record de pluie dans plusieurs régions du Québec [Gouvernement du Québec]. https://www.environnement.gouv.qc.ca/climat/Faits-saillants/2025/septembre.htm.
Meyer, K.M., Macalady, J.L., Fulton, J.M., Kump, L.R., Schaperdoth, I., Freeman, K.H., 2011. Carotenoid biomarkers as an imperfect reflection of the anoxygenic phototrophic community in meromictic Fayetteville Green Lake: biomarkers of anoxygenic phototrophs. Geobiology 9 (4), 321–329. https://doi.org/10.1111/j.1472-4669.2011.00285.x.
Ministère de l'Emploi et de la Solidarité Sociale (MTESS), 2024. M-13.1 Loi sur les mines. https://www.legisquebec.gouv.qc.ca/fr/document/lc/m-13.1.
Ministère de l'Environnement et de la Lutte contre les Changements Climatiques de la Faune et des Parcs (MELCCFP), 2013. *Atlas public – PACES Outaouais – cartes MDDELCC*. Atlas Public – cartes MDDELCC (PACES-OUT). https://www.pes1.enviroweb.gouv.qc.ca/AtlasPublic/CartesPubliques/cartesmddelcc.html?cfg=PacesOUT.json.
Ministère des Ressources Naturelles et des Forêts (MRNF), 2025. Plan De Travail 2025-2026 – Restauration Des Sites Miniers Abandonnés. MRNF. https://mrnf.gouv.qc.ca/wp-content/uploads/PL_travail_restauration_sites_2025-2026.pdf.
Ministère des Ressources naturelles et des Forêts du Québec, 2026. Sigéom – Fiche gîte ou occurrence (Numéro 7622). SIGÉOM. https://sigeom.mines.gouv.qc.ca/signet/classes/I1103_index?format=COMPLET&type_reqt=U&mode=NOUVELLE&l=F&entt=GNM&numr_utls=37948360513&alias_table_crit=F4E16&mnen_crit=NUMR_INTER&oper_crit=EGAL&valr_crit=7622.
Mugova, E., Wolkersdorfer, C., 2022. Density stratification and double-diffusive convection in mine pools of flooded underground mines – a review. Water Res. 214, 118033. https://doi.org/10.1016/j.watres.2021.118033.
Munnoch, K., Renaud, S., Connors, K., 2011. The development of a pit lake at Agrium Kapuskasing Phosphate Operations – an integrated geotechnical, geochemical and biological approach. Mine Closure 2011. Proceedings of the Sixth International Conference on Mine Closure, pp. 545–554. https://doi.org/10.36487/ACG_rep/1152_57_Renaud.
Nürnberg, G.K., 1984. The prediction of internal phosphorus load in lakes with anoxic hypolimnia. Limnol. Oceanogr. 29 (1), 111–124. https://doi.org/10.4319/lo.1984.29.1.0111.
OECD, Organisation for Economic Co-operation and Development, 1982. Eutrophication of Waters: Monitoring, Assessment and Control, 154. OECD Publishing. https://lakes.chebucto.org/TPMODELS/OECD/OECD1982.pdf.
Olive, P., Boulègue, J., 2004. Étude biogéochimique d'un lac méromictique: le lac Pavin, France/Biogeochemical study of a meromictic lake: pavin lake, France. Géomorphol. Relief, Process. Environ. 10 (4), 305–316. https://doi.org/10.3406/morfo.2004.1226.
Omaly, N., 1968. Le lac Pavin. Historique et hydrobiologie. Rev. Sci. Nat. Auvergne 34, 7–31.
Ontario Ministry of Northern Development, Mines and Forestry. (n.d.). Mineral occurrence Database—ArcGIS web application. Retrieved December 3, 2025, from https://mndm.maps.arcgis.com/apps/webappviewer/index.html?id=66ee0efe4d3c4816963737dbdb890708.
Parkhurst, D., Appelo, C., 2013. Description of input and examples for PHREEQC Version 3- A Computer Program for speciation, Batch-Reaction, one-dimensional transport, and inverse geochemical calculations. Techniques and Methods, p. 497. Book 6, Chap. A43]. https://pubs.usgs.gov/tm/06/a43/.
Patton, C.J., Kryskalla, J., 2003. Methods of analysis by the U.S. Geological Survey National Water Quality Laboratory-Evaluation of alkaline persulfate digestion as an alternative to Kjeldahl digestion for determination of total and dissolved nitrogen and phosphorus in water. https://doi.org/10.3133/wri034174.
Pellicori, D.A., Gammons, C.H., Poulson, S.R., 2005. Geochemistry and stable isotope composition of the Berkeley pit lake and surrounding mine waters, Butte, Montana. Appl. Geochem. 20 (11), 2116–2137. https://doi.org/10.1016/j.apgeochem.2005.07.010.
Phillips, R., 2017. Cantley's History. *the Echo of Cantley*.
Piper, A.M., 1944. A graphic procedure in the geochemical interpretation of water-analyses. EOS Trans. Am. Geophys. Union 25 (6), 914–928. https://doi.org/10.1029/TR025i006p00914.
Piper, A.M., 1953. A graphic procedure in the geochemical interpretation of water analyses. U.S. Geological Survey Ground-Water Notes Geochemistry 12, 1–14.
R Core Team, 2023. R: a Language and Environment for Statistical Computing. R Foundation for Statistical Computing. https://www.R-project.org/.
Règlement sur la qualité de l'eau potable. Q-2, r.40. https://www.legisquebec.gouv.qc.ca/fr/document/rc/q-2,%20r.%2040.
Rickard, D., 1997. Kinetics of pyrite formation by the H2S oxidation of iron (II) monosulfide in aqueous solutions between 25 and 125°C: the rate equation. Geochem. Cosmochim. Acta 61 (1), 115–134. https://doi.org/10.1016/S0016-7037(96)00321-3.
Roesler, A.J., Gammons, C.H., Druschel, G.K., Oduro, H., Poulson, S.R., 2007. Geochemistry of flooded underground mine workings influenced by bacterial sulfate reduction. Aquat. Geochem. 13 (3), 211–235. https://doi.org/10.1007/s10498-007-9017-9.
RStudio Team, 2024. *RStudio: integrated development environment for R* [RStudio, PBC]. http://www.rstudio.com.
Révész, K., Qi, H., Coplen, T.B., 2012. Determination of the $\delta^{34}S$ of sulfate in water; RSIL lab code 1951. In: Révész, K., Coplen, T.B. (Eds.), Methods of the Reston Stable Isotope Laboratory: Book 10. U.S. Geological Survey, p. 33. https://pubs.usgs.gov/tm/2006/tm10c10/tm10c10.pdf (Original work published 2006).
Sabina, A.P., 1987. Rocks and minerals for the collector, Hull-Maniwaki, Quebec, Ottawa-Peterborough, Ontario (41), 41. https://doi.org/10.4095/122460.
Seebach, A., Dietz, S., Lessmann, D., Knoeller, K., 2008. Estimation of lake water—Groundwater interactions in meromictic mining lakes by modelling isotope signatures of lake water. Isot. Environ. Health Stud. 44 (1), 99–110. https://doi.org/10.1080/10256010801887513.
Sánchez-España, J., Pamo, E.L., Diez, M., Santofimia, E., 2009. Physico-chemical gradients and meromictic stratification in Cueva de la Mora and other acidic pit lakes of the Iberian Pyrite Belt. Mine Water Environ. 28 (1), 15–29. https://doi.org/10.1007/s10230-008-0059-z.
Søndergaard, M., Jensen, J.P., Jeppesen, E., 2003. Role of sediment and internal loading of phosphorus in shallow lakes. Hydrobiologia 506–509 (1–3), 135–145. https://doi.org/10.1023/B:HYDR.0000008611.12704.dd.
Spence, H., 1929. Mica. Canada Department of Mines. Mines Branch. No. 701; p. 142.
Stoecker, D.K., Hansen, P.J., Caron, D.A., Mitra, A., 2017. Mixotrophy in the Marine Plankton. Ann. Rev. Mar. Sci 9 (1), 311–335. https://doi.org/10.1146/annurev-marine-010816-060617.
Telmer, K., Veizer, J., 2000. Isotopic constraints on the transpiration, evaporation, energy, and gross primary production Budgets of a large boreal watershed: ottawa River Basin, Canada. Glob. Biogeochem. Cycles 14 (1), 149–165. https://doi.org/10.1029/1999GB900078.
Thiel, J., Byrne, J.M., Kappler, A., Schink, B., Pester, M., 2019. Pyrite formation from FeS and $H_2$ S is mediated through microbial redox activity. Proc. Natl. Acad. Sci. 116 (14), 6897–6902. https://doi.org/10.1073/pnas.1814412116.
Vasil'chuk, Y.K., Frolova, N.L., Kasimov, N.S., Winde, F., Budantseva, N.A., Chizhova, J. N., Efimova, L.E., Krasnova, E.D., Terskaya, E.V., Tokarev, I.V., Vasil'chuk, A.C., 2018. Isotope stratification of meromictic Lake Trekhtzvetnoe at the White Sea coast (Russia). Annales de Limnologie - International Journal of Limnology 54, 23. https://doi.org/10.1051/limn/2018012.
Vernon, R.H., 2004. A Practical Guide to Rock Microstructure, first ed. Cambridge University Press. https://doi.org/10.1017/CBO9780511807206.
Von Gunten, K., Warchola, T., Donner, M.W., Cossio, M., Hao, W., Boothman, C., Lloyd, J., Siddique, T., Partin, C.A., Flynn, S.L., Rosaasen, A., Konhauser, K.O., Alessi, D.S., 2018. Biogeochemistry of U, Ni, and as in two meromictic pit lakes at the Cluff Lake uranium mine, northern Saskatchewan. Can. J. Earth Sci. 55 (5), 463–474. https://doi.org/10.1139/cjes-2017-0149.
Wetzel, R.G., 2001. Limnology: Lake and River Ecosystems, third ed. Academic Press. https://doi.org/10.1016/C2009-0-02112-6.

White, I., 1997. The Nature of perkins-sur-le-lac, p. 30. https://static1.squarespace.com/static/54593705e4b006c7bb9ca5f6/t/550086a2e4b072cec00bf157/1426097826346/under_our_feet_eng_print_version.pdf.

Wolkersdorfer, C., Nordstrom, D.K., Beckie, R.D., Cicerone, D.S., Elliot, T., Edraki, M., Valente, T., França, S.C.A., Kumar, P., Lucero, R.A.O., Soler I Gil, A., 2020. Guidance for the integrated use of hydrological, geochemical, and isotopic tools in mining operations. Mine Water Environ. 39 (2), 204–228. https://doi.org/10.1007/s10230-020-00666-x.

Zieliński, M., Szczucińska, A., Drożdżyński, M., Frankowski, M., Pukacz, A., 2019. Water quality assessment of a Meromictic Lake based on physicochemical parameters and strontium isotopes (87Sr/86Sr) analysis: a case Study of Lubińskie Lake (Western Poland). Water 11 (11), 2231. https://doi.org/10.3390/w11112231.